EFFECTS OF OVARIECTOMY AND ANATOMICAL POSITION ON THE COMPACT BONE AS SEEN IN THREE MONTH SUMMER OVINE MODEL

A Thesis

presented to

the Faculty of California Polytechnic State University,

San Luis Obispo

In Partial Fulfillment

of the Requirements for the Degree

Master of Science in Biomedical Engineering

by

Bryan Kraft

June 2014

COMMITTEE MEMBERSHIP

TITLE:	Effects of Ovariectomy and Anatomical Position on The Compact Bone As Seen In Three Month Summer Ovine Model
AUTHOR:	Bryan Kraft
DATE SUBMITTED:	June 2014
COMMITTEE CHAIR:	Scott Hazelwood, PhD Professor of Biomedical Engineering
COMMITTEE MEMBER:	Lanny Griffin, PhD Professor of Biomedical Engineering
COMMITTEE MEMBER:	Clifford Les, DVM PhD Adjunct of Biomedical Engineering

ABSTRACT

Effects of Ovariectomy and Anatomical Position on the Compact Bone As Seen In Three Month Summer Ovine Model

Bryan Kraft

The purpose of this study is to characterize the compact-bone remodeling response to an ovariectomy model of human postmenopausal osteoporosis. Animal models are a beneficial practice allowing for the evaluation of the effectiveness of medical therapies and devices on diseases. The ovine model was chosen for this study due to its large size, similar bone remodeling to humans, and cost effectiveness. The main obstacle to overcome with the use of the ovine model was the lack of natural menopause experienced by this species. To overcome this, it was necessary to perform an ovariectomy to create estrogen depletion and artificially induce menopause in the sheep. The use of OVX (ovariectomized) sheep has been widely accepted as a model for the loss of bone mass. Effects of bone loss first appear around 3 months post-ovariectomy, however the effect of the bone loss at the 3 month time point as well as its effect on different anatomical positions within the bone have not been thoroughly studied. 16 skeletally mature Columbia- Rambouillet cross ewes were used for this portion of the study. The group of 16 was divided into 2 groups, one underwent an ovariectomy procedure and the other group underwent a sham surgery to put them through the same surgical stress as the test group. 3 months post surgery the ewes were sacrificed and had their right and left radii and ulna removed. The left radial-ulna bone was then divided into 6 anatomical locations: craniolateral, cranial, craniomedial, caudolateral, caudal, and caudomedial. With the bone divided into different anatomical sectors, microradiographs were fabricated to allow for further analysis of the bone samples. Using the microradiographs histomorphometric measurements were taken to quantify the bone remodeling occurring; the measurements taken were the bone volume to tissue volume, fraction of remodeled tissue and material, the millimeter (mm) of cement line per square mm of bone tissue and material,

Osteons per mm^2, and the mean osteon area. Densitometry analysis was also performed using the microradiographs using image analysis and the use of an aluminum step wedge on each microradiograph as a key. Once all of the data was collected a 2-way repeated measures ANOVA statistical analysis was performed on the histomorphometry and densitometry data to evaluate the possible differences seen due to treatment, anatomical sector, and possible interaction of both. For the histomorphometry portion there was a significant variation seen between the caudal sectors of bone in the OVX vs control sheep in both the fraction of remodeled material and the mean osteonal area. There was also a significant variation seen between the caudomedial sectors of bone in the OVX vs control sheep for the average Osteons per mm^2. For the densitometry analysis it was found that the OVX sheep had significantly lower bone density than the control sheep. This study shows that there are significant changes seen even after only 3 months with depleted estrogen levels and that differences can be seen based on the anatomical sector of the bone. With this information it will be important to take this into consideration when creating future studies using the ovariectomized ewe as an animal model for postmenopausal osteoporosis study.

ACKNOWLEDGMENTS

I would like to thank Dr. Scott Hazelwood for his support and guidance through this project. I would also like to thank Dr. Clifford Les for introducing me to the project and for the support throughout.

TABLE OF CONTENTS

LIST OF TABLES

LIST OF FIGURES

1. Introduction

1.1 Purpose

More than 75 million people in the United State, Europe, and Japan are affected by osteoporosis [1]. Osteoporosis is defined by a decrease in bone mass and alteration to bones micro-structure increasing the bone fragility leading to increased risk of bone fracture [2]. Estimates suggest that nearly half of women over the age of 50 will break a bone due to osteoporosis in their lifetime [3] The National Osteoporosis Foundation (NOF) states that the only way to detect osteoporosis before a bone fracture occurs is by the use of a bone density test. The best current known bone density test is duel energy x-ray absorptiometry (DEXA) [3]. Typical DEXA tests will test the hip, wrist, and spine and report results using T-scores. A normal bone density will result in a T-score of -1 or higher, a test that suggests osteoporosis will result in a T-score of -2.5 or lower [3]. Osteoporosis increases the risk of fracture, particularly the spine, wrist, humerus, and pelvis. In the year 2000 there was an estimated 5.8 million disability adjusted life years (DALY's) attributed to osteoporotic fractures alone [4]. With osteoporosis being such a major health threat to such a large population it is necessary to understand the mechanisms behind it to better improve our treatments as well as how to properly test these treatments with improved animal models. To reach this step the anatomy of bone must be discussed to better understand osteoporosis.

1.2 Skeletal Biomechanics

1.2.1 Architecture of Bone

Bone is essential to the body, it provides structural support for all other components of the body, provides a framework for motion since our muscles need to pull

on some rigid body to create motion, offers protection from brunt trauma, acts as a calcium repository, and houses the marrow, the tissue that produces blood cells and stem cells in the body [5]. The architecture and shape of bones among vertebrate skeletons are fairly conservative and stereotypical [6]. With this knowledge it can be seen that at a macro level we can usually recognize a femur or a tibia regardless of what animal it came from even though there is still quite a varied skeletal morphology amongst vertebrates [6]. It would seem that bones amongst a species are somewhat static structures within a given species at the macro level [6]. However, once looked at on a scale of microns to millimeters, bone becomes a highly dynamic tissue [6].

Once we look at bones as dynamic structures we can begin to understand their varying shapes and types. Bones are able to sense mechanical loads that are applied to them, and are able to modify their structures to adjust to these loads appropriately; this principle is known as Wolff's Law [6]. Bone is a very unique material because of its ability to have high stiffness in certain directions yet be flexible in others due to its material composition and structure [7]. With bone’s ability to be flexible, it is able to absorb energy and conform to loads put on it from the environment [7].

Bone is made up of two different types of bone tissue, cortical bone and trabecular bone. Cortical bone is the stronger/heavier type of bone with a low porosity, typically less than 10% [5]. This bone type is typically found in the shafts of long bone bones and the general outer layer of most bones. Cortical bones microarchitecture is essential to understanding its mechanical properties. Cortical bone tissue is laid down in layers 5 um thick known as lamellae [5]. Within the lamellae collagen fibers run parallel to each other, but the orientation of neighboring layers differs, much like many composite

materials [5]. The arrangement of lamellae also differs from the outer and inner surfaces compared to the space in between. The outer surfaces are circumferentially arranged around the bone parallel to one another [5]. The tissue in between the outer and inner layers is made up of osteonal bone, which consists of cylindrical structures formed by concentric lamellae approximately 200 μm in diameter aligned with the long axis of the bone [5]. This solid bone matrix is permeated by an intricate network of canals to provide nutrients to the osteocytes trapped in the bone matrix, the central Haversion canals and surrounding lamellae make up what is called an osteon seen in Figure 1[6].

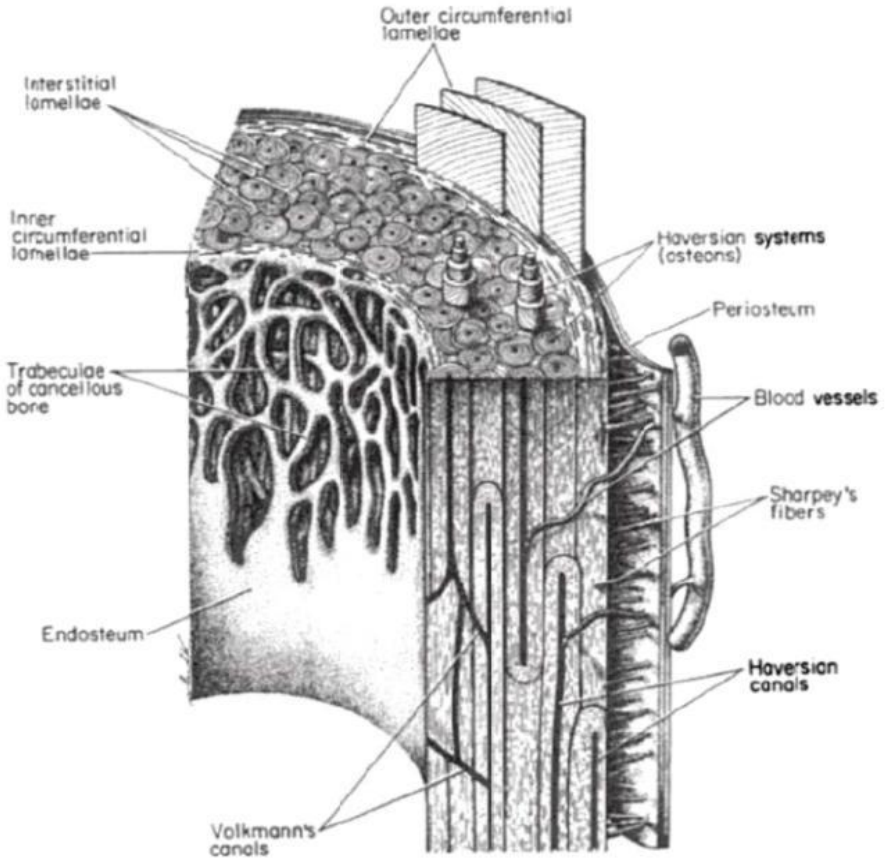

Figure 1 Important features of cortical bone [6]

Trabecular bone, also known as cancellous bone, is found in the vertebrae and the ends of long bones. Since many age related fractures occur in trabecular bone sites, such as the proximal femur, distal radius, and vertebral bodies, it becomes even more important to study this type of bone [5]. Trabecular bone is much more porous than cortical bone at about 75 – 90% porosity and is made up of a network of interconnecting struts called trabeculae [6]. These trabeculae are formed in much the same way as cortical bone with lamellae running in parallel to the trabeculae. Trabecular bone's structure is somewhat weaker than cortical bone, however is much lighter due to its much higher porosity [5]. Typical trabeculae in healthy bone have an average thickness of 200μm; in osteoporosis patients it is seen that there are fewer trabeculae and that they become thinner, this will be discussed further later in the paper [5].

With further examination of cortical bone and trabecular bone it can be characterized as primary or secondary bone. Primary bone is the bone tissue initially laid down on the periosteal surface during growth. Primary bone is typically in the form of circumferential lamellar bone, where the lamellae are parallel to the bone surface [6]. Blood vessels are incorporated into the lamellar structure surrounded by multiple circular lamellae forming the primary osteons and osteonal canals in the bone. The other type of bone tissue is secondary bone, which results from the resorption of existing bone and replacement with new bone, the process known as remodeling [6]. Most secondary bone tissue in cortical bone consist of cylindrical structures known as secondary osteons that are about 200um thick much like primary osteons. These new secondary osteons however leave a noticeable boundary called a cement line [6]. In adult humans, most compact bone and almost all trabecular bone is composed of secondary bone with some remnants

of primary osteons that have been only partially resorbed as seen in Figure 2, this is due to the continual remodeling and repairing of the bone over one's lifetime [8].

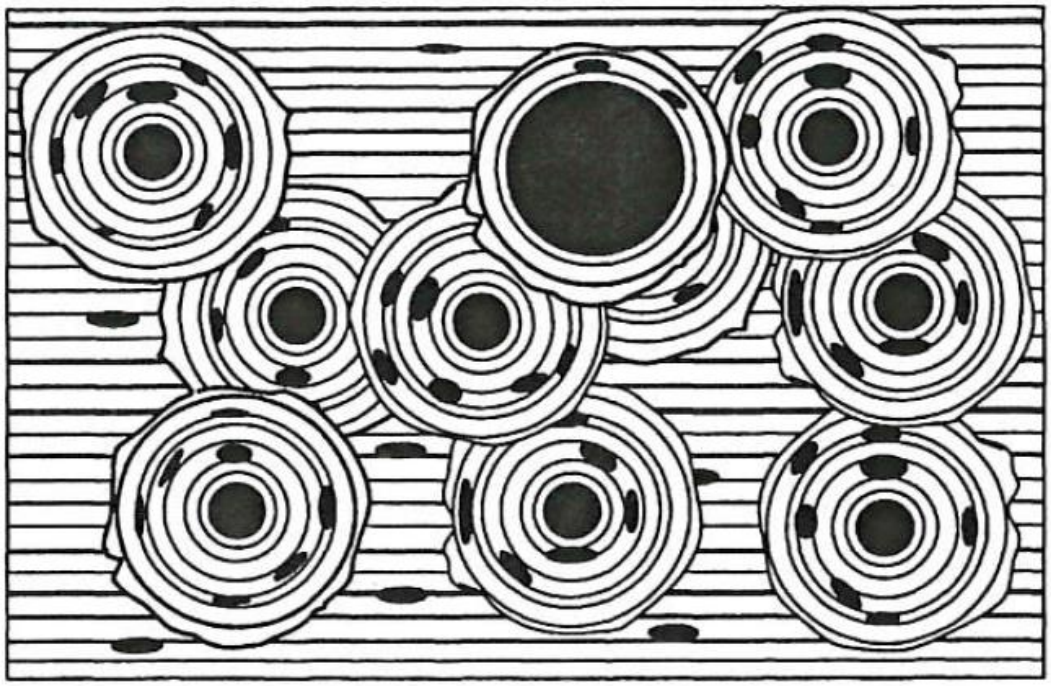

Figure 2 Schematic diagram of secondary osteons within an area of primary bone. [6]

1.2.2 Biomechanical Properties of Bone

The material that bone is made from is as important to the biomechanics of bone as is the shape and structure of bone. Bone like other connective tissues consists of cells and organic extracellular matrix of fibers and ground substance produced by cells. However, bone is unique because it has a high content of inorganic materials, in the form of mineral salts [8]. In normal human bone the inorganic portion consist primarily of calcium and phosphate similar to synthetic hydroxapatite. This inorganic material makes up 60 to 70% of bones dry weight and is what gives it its rigidity and hardness [8]. Along with bone's inorganic material, its organic material is mainly made up of collagen, roughly 90% of all organic material in bone [9], which gives the bone its flexibility and

tensile strength [6]. With bones mix of inorganic and organic materials, it obtains unique mechanical properties, biomechanically bone tissue can be regarded as a biphasic composite material, with the mineral portion as one phase and the collagen and ground material as the second phase [8]. Materials such as bone are mainly a strong, brittle material with a weaker more flexible material embedded in it to create a combined material that is stronger for its weight than either material by itself [8]. Two of bone's most important mechanical properties are its strength and stiffness. These and other characteristics can be best understood by examining its behavior under loading. Putting different loads on the material will cause it to deform, by measuring these deformations a load-deformation curve can be found, much like the example in Figure 3 [8].

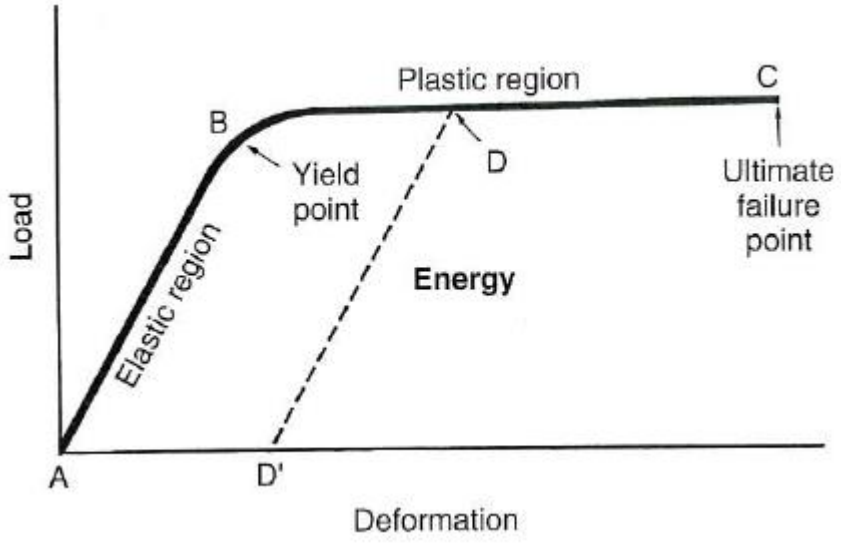

Figure 3 Example of a Load-deformation curve [8]

Information about the bone's strength, stiffness, and other mechanical properties can be found by examining the bone's load-deformation curve. As seen in the curve the first straight portion is the elastic region, where the bone will return to its initial state after the load is taken off the bone. Once the load is enough to go past the yield point the

material will be permanently deformed to some extent and at a certain load will reach the ultimate failure point, at which the bone will fracture. There are three parameters for determining the strength of a structure that are reflected on the load-deformation curve: 1, the load the structure can sustain before failure (the ultimate failure point); 2, the deformation that can be sustained before failure; and 3, the energy than can be stored before failure (area under the curve) [8]. The load-deformation curve is a great way for determining the mechanical properties of the whole structure, but much like mentioned before, the properties of bone change at the micro scale and it is necessary to look at not only the mechanical properties of the whole bone, but of the mechanical properties of each type of bone and what affects those properties.

The biomechanical properties of bone are determined by its composition and structure at multiple length scales. On a scale of micrometers the tissue behaves like a fiber-reinforced composite with the hydroxyapatite mineral providing stiffness and the collagen fibers providing tensile strength and ductility [8]. Once we begin to look at the different bone types we begin to see differences in their mechanical properties. When looking at an individual trabecular strut it is generally thought to be slightly (20-30%) less stiff than cortical bone tissue owing to subtle differences in mineralization and lamellar structure [5]. Cortical bone has strongly anisotropic properties, specifically stiffness and strength along the bone axis due to the longitudinal alignment of the osteons and orientation of the lamellae [5]. Cortical bone is typically loaded along its axis in compression, so it lends to the fact that cortical bone is stronger in compression than in tension. Bones strength is not only dependent on the strain, but also on the strain rate, where the bone becomes stiffer and stronger at higher strain rates [5]. This gives bone a

similar characteristic to a viscoelastic material, which is a desirable mechanical property to compensate for higher loads imposed by sudden superphysiological loading, such as caused by fall impacts or vigorous activity [5].

The mechanical properties of trabecular bone have a significant variation in stiffness and strength due to these properties being affected by the density and architecture of the bone. To test the properties of trabecular bone, a specimen with dimensions > 1mm is analyzed for its "apparent" mechanical properties. These properties depend on the bone tissue matrix, amount of tissue, and the structural organization of the trabeculae which vary with anatomic site, age, and disease [5]. A typical stress-strain curve for trabecular bone of different relative densities can be seen in Figure 4 [5].

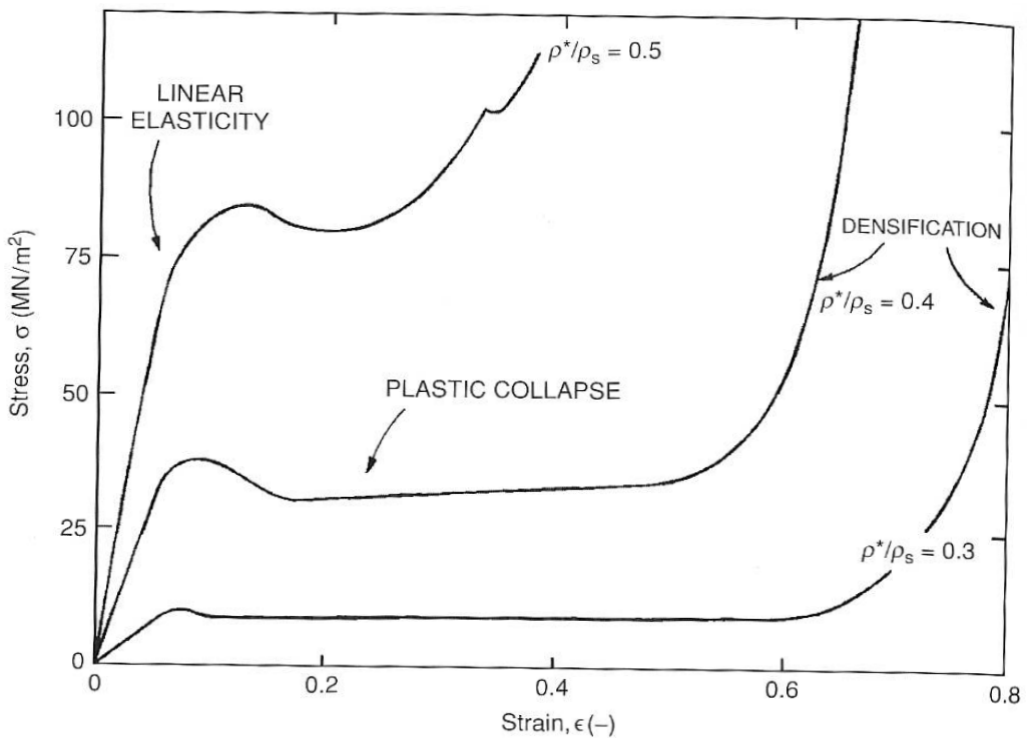

Figure 4 Compressive stress-strain curves of trabecular bone of different relative densities [5].

As seen in the figure trabecular bone acts like a linearly elastic material at small strains, but then enters a large anelastic region as the trabecular rods and plates collapse under the increasing strain. Once the pores within the bone are eliminated by collapsing of the trabeculae, the trabeculae begin to run into each other causing a steep rise in the stress. With the collapse of the trabeculae, trabecular bone absorbs a high amount of energy allowing the bone to undergo large compressive strains without high stress [5]. The relative density of trabecular bone strongly affects the mechanical properties of the bone which can be seen when the Young's modulus or compressive strength is plotted against the apparent density, as shown in Figure 5 [5].

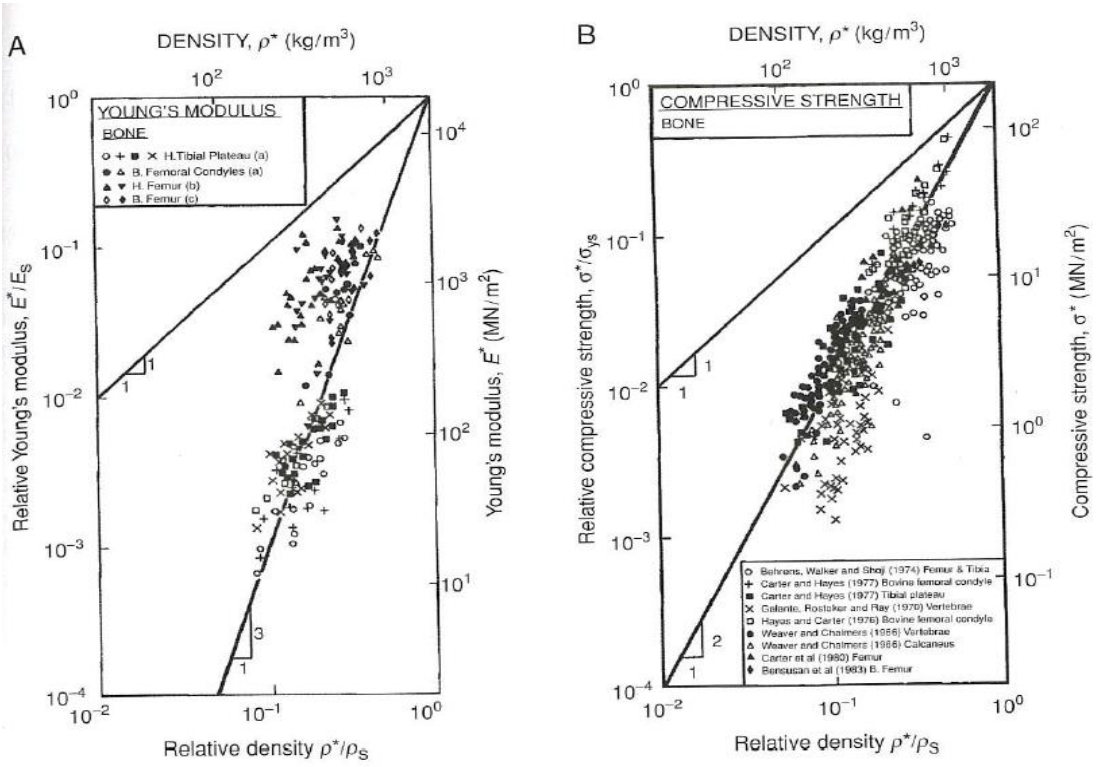

Figure 5 Relationship between relative density and Young's modulus (A) or compressive strength (B) of trabecular bone [5].

1.2.3 Analysis of Skeletal Biomechanics

A more accurate measurement of key material properties of bones is essential to better understand the material properties behind bones and to better predict the chances of fractures in patients. Several noninvasive bone mass measuring techniques exist and mostly depend on the absorption of photons by the bone since the mineral makeup of bone is more prone to absorbing photons than the soft tissues, collagen, and water contained in the bone [7]. Prior to the 1970's the simplest way to test bone density was the use of radiographic films “x-rays”. However, this method used significant radiation doses and could have a perceived reduction in bone density of 30-50% due to the variability in exposure and processing [7]. In the 1970's a better solution was found, called photon absorptiometry, which involves scanning across a bone with a beam of photons emitted by a low-level radionuclide and a detector opposite of the beam. This method significantly reduced the radiation exposed to the patient and increased the accuracy. The system works by being able to record the intensity of the radiation coming through the material and knowing the total thickness of the material to produce a curve that is proportional to the mineral content of the bone [7]. Later the use of two photon beams with different absorption coefficients would correct for the small amounts of photons being absorbed by soft tissue giving it even further accuracy. In the 1990's an alternate version was implemented that substituted the radionuclide source with a low energy x-ray, known as dual energy x-ray absorptiometry (DEXA). This method allows for us to be able to scan the whole body for its bone mineral content noninvasively with accuracy within 1-2% [7]. The use of microcomputed tomographic scanning (micro-CT) has become another accurate method of obtaining three-dimensional measurements of bone stereology, volume, and micro architecture in the evaluation of membranous bone;

however it is limited to a small section [10].

Another commonly used method for analysis of bone structure and composition is stereology. Stereology is a method of exploring a three-dimensional space, when only two-dimensional sections through solid bodies are available [7]. This method is often used to determine apparent density and calculating porosity. Stereology uses histological cross sections viewed under a microscope and measures the void volume fraction from the two-dimensional image. There are a few different methods of measurements used to obtain this information. One such method is the use of a "zero-dimensional" technique, where a grid of points is placed over the image and the fraction of points that fall on the voids is recorded [7]. There have been specific types of grids created of this purpose, one such grid that is often used is a Merz grid, seen in Figure 6.

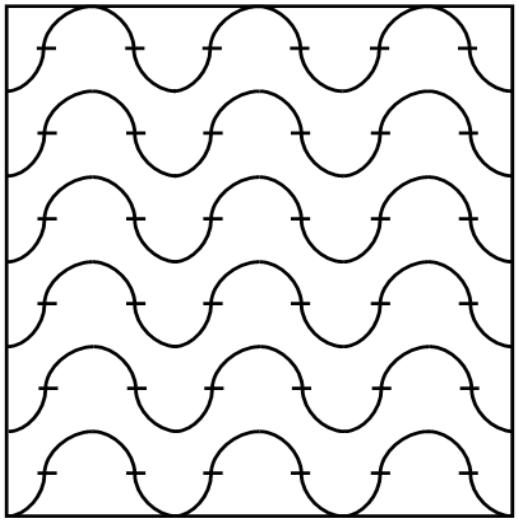

Figure 6 Merz Grid formed by 36 hash marks on 6 evenly spaced hemicicular lines

The Merz grid consist of 36 point markings and 6 hemicircular lines, this grid would be placed in either the eye piece of the microscope being used or superimposed over an enlarged image of the specimen. Using this style of grid the number of points that

intersect voids in the cross section of the material in question would be point counted, where P_v is the points that intersected the voids and P_t is the total number of points on the grid. Using these recorded values a simple ratio for porosity is found (Equation 1).

$$Porosity = P_v / P_t \quad \textit{(Eq. 1)}$$

This ratio can then be used in other calculations to obtain key histomorphometric measurements for the bone surfaces.

1.3 Bone Remodeling

1.3.1 Remodeling and Resorption

As bone grows during childhood into adulthood it needs not only to grow in size and length, but be shaped in various ways. The initial increased growth in bone occurs when new bone is deposited by osteoblasts without previous bone resorption [11]. However, with increasing size the bone needs to maintain its shape and structure requiring removal of bone in certain areas and adding it in others. Bone also needs to repair itself from fatigue damage and adjust the architecture of the bone as the load conditions change over one's lifespan. Bone remodels itself through the coupled removal of old bone and its replacement through the synthesis of new bone matrix and its subsequent mineralization [12]. Bone does this by involving osteoclastic activity to resorb damaged or unnecessary bone and osteoblastic activity to form new bone [7]. For the purposes of this paper we will focus on the remodeling actions of bone. Remodeling refers to the actions of osteoclast and osteoblasts working in the same site of damaged bone, removing old bone and replacing it with new bone [7]. The process of remodeling repairs microscopic damage within the bone increasing its mechanical efficiency and preventing the accumulation of fatigue damage that could lead to fatigue fractures [7].

This remodeling process is completed by a group of osteoclast and osteoblast working together in basic multicellular units, also known as BMU's. A BMU is made up of roughly 10 osteoclast and several hundred osteoblasts [7]. BMU's have a typical lifetime that has been broken down into three principle stages: activation, resorption, and formation (ARF). The activation occurs when a chemical or mechanical signal causes osteoclast to form and begin to remove the specified section of bone. These osteoclasts resorb the targeted bone leaving behind a tunnel or trench of approximately 200μm in diameter for a varying distance [7]. Osteoblasts then follow at a slower rate, replacing the removed bone. The specifics of this process will be discussed in further detail below. With the BMU creating a tunnel through the compact bone it creates a new osteon. The front end of the BMU contains a capillary "bud" to supply nutrients for the osteoclast and osteoblast. Inherently BMU's become isolated within the cortex of the bone and require continual vascular supply causing the tunnel to not be completely filled in creating a new Haversian canal to allow for the vessels. The osteoblasts that become buried in the bone after remodeling are referred to as osteocytes and are interconnected with other osteocytes throughout the bone via canaliculi, small tunnels [7].

1.3.2 Analysis of the ARF Sequence

Remodeling is the primary determinant of the mechanical properties of bone, their resistance to fatigue failure, and their ability to adapt to changing mechanical environments [7]. By understanding the remodeling process we can better understand its effects on skeletal tissue mechanics. Once we have this knowledge then we can create methods used to quantify bone remodeling and how it actually affects the bone structure.

As stated above the remodeling process revolves around the BMU and the process

it follows during remodeling. The BMU remodeling sequence follows well defined phases that begin with activation, followed by resorption, then finally formation. This is known as the A-R-F sequence and can be depicted in the schematic diagram seen in Figure 7(fig 3.1[7]) [7].

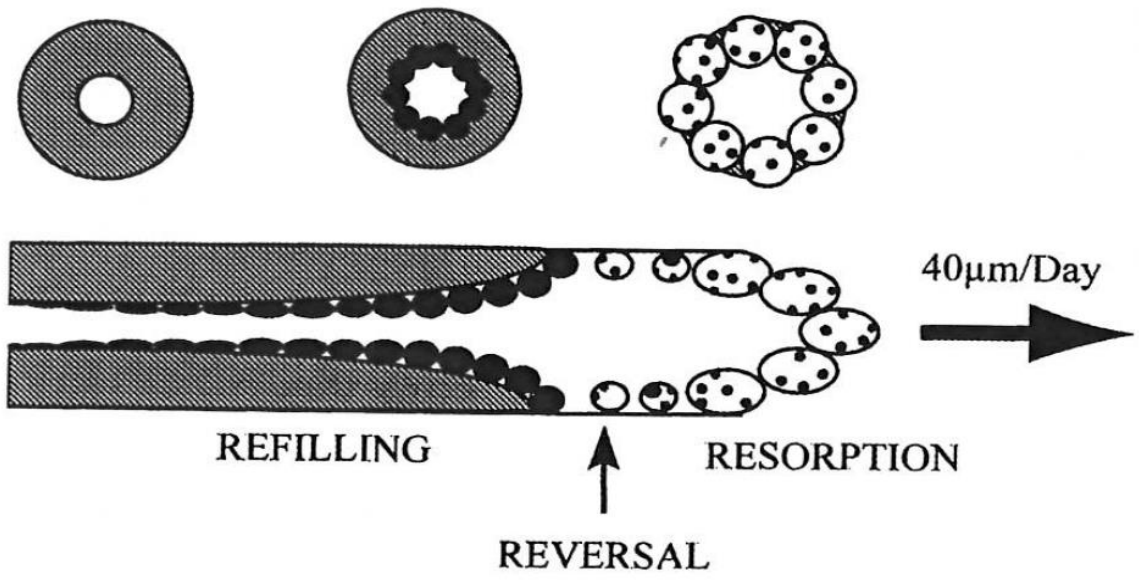

Figure 7 Schematic diagram of an osteonal BMU. Larger, multinucleated cells to right are osteoclast; smaller cells shown in black to left are osteoblast [7]

The A-R-F process can be broken down even further than just activation, resorption, then formation, but into 6 phases.

First, it starts with activation where differentiated cells must be recruited from precursor cell populations before any resorption or bone formation can occur [7]. This process typically takes 3 days to produce the osteoclast to begin the origin of the BMU [7]. Activation is not completely understood, however there are a few main principles that have been the key points of research for what causes the activation of bone remodeling. First is that bone may contain sensor cells that monitor mechanical strain. It has been

shown that when mechanical stimulus is too low, remodeling removes bone and when the stimulus is too high, remodeling adds bone [13]. Second, it has been suggested that osteocytes act as bones mechanosensing cells since they are distributed throughout the bone matrix. It is also known that osteocytes communicate with each other as well as osteoblasts and that they can sense mechanical changes through stretch-activation channels, flow of the interstitial fluid, and electrical potentials [14]. Third, is that osteocytes may sense fatigue damage and transmit signals activating remodeling to remove and repair this damaged bone [13]. The final concept is that cells of osteoblast lineage control the initiation of remodeling, many have hypothesized bone lining cells, previously osteoblasts, are responsible for activating BMU's to remodel bone in response to signals given by osteocytes or hormones [13].

Once the activation phase is completed the newly formed BMU begins the resorption phase. Osteoclast move longitudinally at a rate of about 40μm/day in the rough shape of a cone with an ellipsoidal surface of approximately 200μm in diameter and about 300μm long [7]. This phase goes on for a few days resorbing bone in its path before the next phase, called reversal, begins. Reversal is the transition from osteoclastic to osteoblastic activity where new bone is formed. The boundary of a completed secondary osteon is the cement line also referred to as the reversal line, indicating where the transition phase takes place [7]. The total time for the resorption and reversal phases takes about 30 days.

Once the reversal phase is completed osteoblasts appear around the periphery of the tunnel formed by the osteoclasts during the resorption phase and begin refilling the cavity, starting the formation phase [7]. Concentric lamellae are laid down by the

osteoblasts to fill in the resorbed region. The rate at which the lamellae is placed decreases as the refilling progresses averaging at about 1-2 μm/day, this is considerably slower than the resorption phase [7]. As it was stated earlier the tunnel is not filled completely to allow for a vascular loop to nourish the osteoblasts and osteoclasts during the ARF sequence. The tunnel that is left behind, called the Haversian canal, is typically 40-50μm in diameter. These vessels also aid in transport of calcium and phosphorus to and from the bone when necessary [7]. The formation phase in an adult human takes about 3 months to complete [7].

Following the formation phase is the mineralization phase. This phase takes place after most of the unmineralized organic material has been deposited into the bone matrix during the formation phase. There is a delay of about 10 days, known as the mineralization lag time, resulting in a layer of osteoid between the osteoblast and the mineralization bone [7]. During this phase mineral is deposited within and between the collagen fibers found in the new bone. Roughly 60% of the mineralization occurs within the first few days, this is known as the primary mineralization. The remaining 40%, secondary mineralization, is added at a decreasing rate taking another 6 months to complete [7]. This is essential to the understanding of the bones mechanical properties, because the properties of incompletely mineralized osteons can vary by large amounts as compared to completed (older) osteons.

The final phase of the the A-R-F sequence is the quiescene, where the osteoclasts disappear from the region, and the trapped osteoblasts become osteocytes or Haversion lining cells [7]. The newly formed bone then carries on their usual mechanical, metabolic, and homeostatic functions [7].

1.3.3 Measurement of Osteonal Remodeling

Along with understanding the remodeling sequence of bone it is important to use this knowledge to create methods of analysis and measurement of bone remodeling to put it into a quantitative form. By having quantitative analysis of how bones remodel, we can create more accurate treatments for bone diseases and be able to improve bone healing. There already exist multiple methods of analysis currently that are helping us produce new and improved treatments. One type of method is using spatial process algebra, the shape calculus, using levels of Receptor Activator of Nuclear Factor κ B (RANK) and Receptor activator of nuclear factor kappa-B ligand (RANKL) and cellular activity in the body in relation to the BMD during bone remodeling [15]. RANK/RANKL signaling is an important factor affecting bone metabolism. RANK refers to a protein expressed by osteoclasts in bone; RANK is a receptor for RANKL, another protein produced by osteoblasts [15]. This signaling triggers osteoclast differentiation, proliferation, and activation, prominently affecting the resorption phase during bone remodeling [15]. By creating a mathematical comparison of the varying levels of RANKL in one's system and the level of cell activity we can analyze the effects on bone density [15]. This is just one example of how a computational approach can be used to analyze bones ability to remodel under given conditions.

Another method of accurately measuring the amount of bone remodeling in bone is the use of diagnostic imaging tools along with computational and biological variables to accurately measure bone mass densities and the structures of patient's bones. The adequate conjugation of diagnostic imaging tools, DEXA, along with computational numeric simulations may increase the knowledge on bone remodeling and on bone strength [16]. Consistent validation methodologies are mandatory to obtain valid results,

and furthermore the inclusion of patient-specific information, to express the inter-individual geometric and biological variability is also valuable in the computational model [16]. In one such study the methodology proposed represented a partial validation of the bone remodeling model in terms of bone mineral content (BMC) for a specific region, namely the femoral neck [16]. In their study DEXA exams were performed on the femur of Caucasian women of post-menopausal age and a descriptive statistical study of the patients was conducted using their BMD values, age, height, weight, and body mass index (BMI) [16]. A computational model was applied to a three-dimensional finite element model of the proximal femur for 25 values of k, which can be understood as the cost supplied by the human body for bone remodeling depending on age, hormonal status, and disease status [16]. Both methods were then compared and it was found that there is a set of k values that are able to closely predict the mean formal neck BMC [16]. This use of a computational model along with biological variables can accurately predict the BMC to that of the gold standard diagnostic imaging tool, DEXA, with small relative errors. It also allows for new perspective on osteoporosis by being able to simulate multiple variables as compared to DEXA.

The measurement of BMC has been done by the use of DEXA or histomorphometric analysis with the use of microradiographs of histological sections from sacrificed specimens. The option to measure BMC in vivo has been a goal to be able to get these measurements without the sacrifice of a specimen to obtain quantitative analysis of remodeling bone. Recently it has become possible to use micro-computed tomography (mirco-CT) to calculate an objective measurement of the BMC within a sample of bone, based on three-dimensional CT scans of excised or live animals [17].

Micro-CT analysis offers the advantage of precise quantification of mineralization within a defect, and can be acquired in live animals allowing for serial studies of individual animals [17]. The noninvasive micro-CT technique facilitates longitudinal studies and provides quantitative estimates of bone growth with high precision (+/-2.5%)[17]. In vivo micro-CT data is also acquired at adequate spatial resolution (45μm) in a relatively rapid time of 15min, making it a very quick and cost effective approach to monitoring bone remodeling [17].

With having multiple ways to quantify bone remodeling we can now use this information to create new treatments and solutions to bone damage and current bone diseases. By creating faster, more accurate and cost effective analysis methods diseases can be diagnosed and treatment can be done much earlier and more effectively.

1.4 Osteoporosis

Osteoporosis is the result of reduced bone mass and disruption of the micro-architecture of bone, causing decreased bone strength and increasing the risk of fracture. Bone remodeling plays a critical role in the cause and prevention of osteoporosis. Osteoporosis occurs as a result of increased bone breakdown by osteoclasts and decreased bone formation by osteoblasts [4]. This creates a negative balance of bone formation and the amount of bone resorption. As this imbalance increases it leads to excessive bone loss compromising the strength of the bone [11]. An example of the effects of this imbalance us shown in Figure 8 below, where the top image is an electron micrograph of a 31 year old woman’s vertebra and the bottom image is of a 70 year old woman's vertebra. It can be seen that the larger plate like struts have become fewer and much smaller rod like struts connecting the overall bone structure creating a much more

porous micro architecture as compared to the 31 year old's bone.

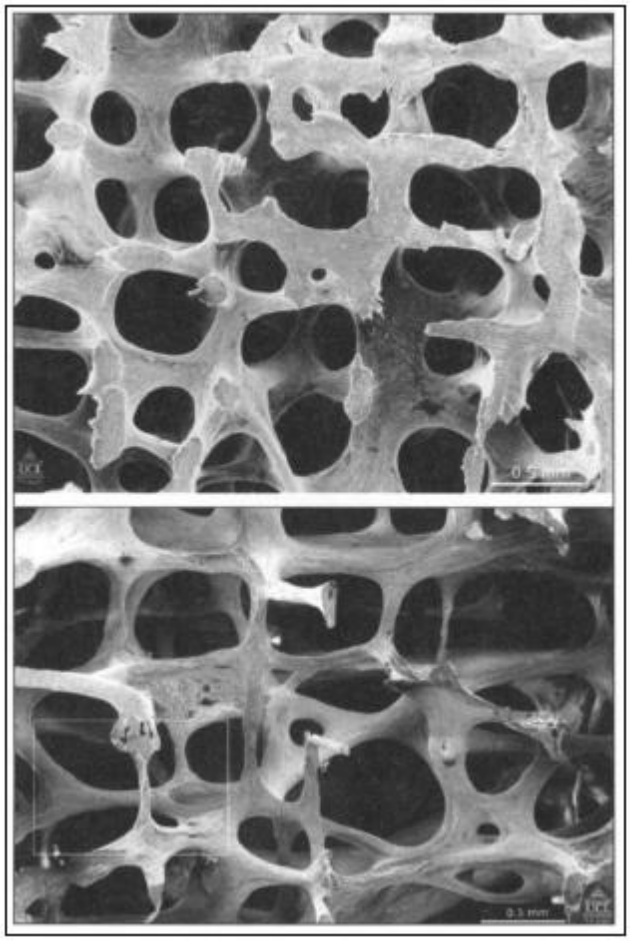

Figure 8 The structure of L3 vertebra in a 31 year old woman (top) and 70 year old woman (bottom) is shown using scanning electron micrographs. Note that many of the plate-like structures have become converted to thin rods [4]

Aging is closely related with bone loss, especially after the age of 50 [4]. With increasing age and bone loss, individuals are more prone to bone fractures of the spine, hip, wrist, humerus, and pelvis. It has been shown that BMD falls significantly due to age-related and menopause-related bone loss [18]. The role of estrogen deficiency in menopausal and age related bone loss in women has been well documented [4]. Osteoporosis is seen in 10.6% of women with menopause of a duration of 0-3 years, 16.2% of women with menopause of duration of 3-7 years, 31.9% of women with

menopause duration of more than 7 years, and a staggering 70% of women over the age of 80 years old [19, 20]. Bone loss also affects men, however the peak bone mass of men is 20 to 30 percent higher than woman's peak bone mass [18]. Along with menopausal and age-related bone loss women are much more susceptible to osteoporosis than men. There are other key factors that may play roles in developing osteoporosis including calcium deficiency, alcoholism, smoking, vitamin D insufficiency, and reduced physical activity with aging [4,18]. Genetic factors also are believed to influence peak bone mass obtained by the third decade of life. Peak bone mass has been shown to significantly affect ones bone mass later in life and is strongly influenced by nutritional intakes and level of physical activity [4].

1.4.1 Postmenopausal Osteoporosis

Menopause occurs in woman between the ages of 40-60 where ovarian function declines and production of hormones for the body's endocrine system decreases. In particular estrogen and progesterone are produced in significantly lower amounts post-menopause. Decreasing estrogen levels have shown to play a key role in increased bone loss early in the postmenopausal period contributing to an increase risk of fracture incidence [21]. There are many different risk factors for the development of osteoporosis as discussed earlier, however estrogen depletion has a direct effect on increased bone loss and is a major factor in leading to osteoporosis in women.

Estrogen has been linked to osteoclast activities in bone remodeling [22]. Estrogen's role in regulating bone loss is connected to the regulation of cytokines that are critical to osteoclast stimulation. Interleukin-1 (IL-1), interleukin-6 (IL-6), and tumor necrosis factor (TNF) are the cytokines regulated by estrogen [22]. These cytokines are

integral in increases in osteoclastogenesis, the osteoclast life span, and also have the ability to stimulate their own synthesis. Estrogen's role in regulation of cytokines: IL-1, IL-6, and TNF production can be seen in Figure 9 [22].

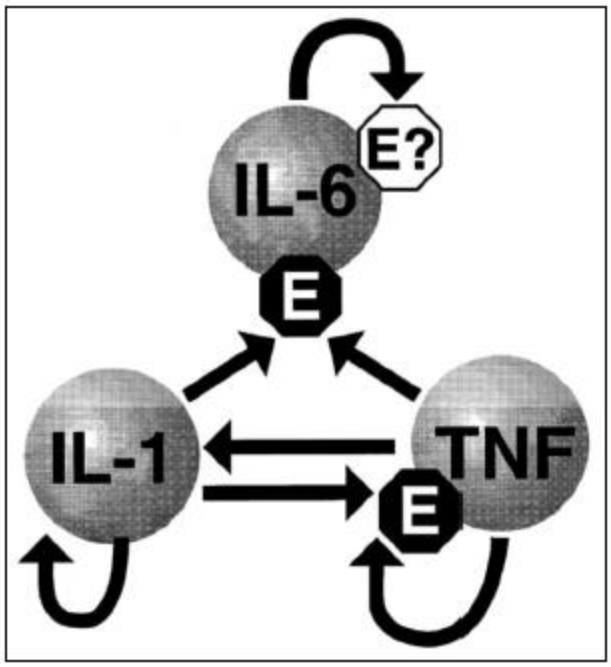

Figure 9 Regulation of IL-1, IL-6, and TNF production. Each arrow indicates a stimulatory effect of a cytokine on its own synthesis, or the synthesis of another cytokine. Demonstrated suppression of the stimulated synthesis of IL-6 and TNF by estrogen ("E") is indicated by filled octagons, and the potential suppression of IL-6 induced IL-6 by estrogen is indicated by an open octagon [22]

With an estrogen deficient environment, IL-6 mediates an increase in osteoclast formation. When estrogen is present it suppresses IL-6, decreasing the amount of osteoclasts being formed [22]. Other cytokines such as transforming growth factor-(β) (TGF-β) inhibits osteoclastogenesis by stimulating osteoclast apoptosis. Estrogen stimulates TGF-β located in osteoblastic cells. With the depletion of estrogen in postmenopausal women it is likely that the levels of TGF-β are decreased while the levels of IL-1, IL-6, and TNF will likely increase. This shift in cytokine levels leads to increased lifespans of osteoclasts [22]. With osteoclast lifespans being increased the level

of bone resorption is also increased causing a greater amount of bone loss as compared to normal conditions [11,22].

1.4.2 Treatment Option for Osteoporosis

Treatments of osteoporosis currently focus on preventing or delaying the onset of osteoporosis by increasing ones peak bone mass and by trying to prevent/slow bone loss caused by aging and menopause. One treatment procedure is through the use of nutritional supplements such as calcium and vitamin D. Calcium and vitamin D are given along with other drugs for osteoporosis to those with low calcium intake and elderly woman to decrease the rate of bone loss [23]. The use of an annual injection of calcium and vitamin D in elderly men and woman has shown trends for reducing non-vertebral fractures by as much as 24%. However, the overall efficacy of using calcium and vitamin D supplements as a treatment for healthy elderly people with sufficient dairy intake and normal BMD has not been established [23].

With menopause and hormone depletion being related with bone loss later in life, hormone replacement therapy (HRT) is another possible treatment to help prevent bone loss. HRT however is a less sought after treatment due to the associated adverse effects. With the decision of using HRT some of the adverse effects taken into account are the unknown risk of increased chance of breast cancer, menstrual bleeding, and other possible gynecologic symptoms [23]. HRT has shown to reduce markers of bone resorption, decrease the rate of bone loss, and decrease incidence of fractures in post-menopausal and osteoporotic women [24]. Several studies have shown that the use of HRT decreases the risk of hip fractures by 30% and a 50% reduction in the risk of spinal fractures [23]. The use of calcium supplements along with HRT is hypothesized to further

improve bone loss reduction and help reduce fracture risk [23]. Once HRT is withdrawn the reduction of fracture risk is lost within 5 years causing an issue of how to optimally time and at what duration to give the treatment [23]. Although HRT has proven to be a viable option of treatment to prevent increased bone loss, the perception of increased risk of breast cancer and other side effects has minimized its adoption as a treatment by the majority of the affected population [24].

Another treatment option is the use of bisphosphonates because of their strong affinity for bone apatite, being a potent inhibitors of bone resorption by reducing the recruitment and activity of osteoclasts, and the ability to be artificially synthesized with relative ease [23]. Studies have shown an increase in bone wall thickness in humans and nonhuman primates after long term treatment with bisphosphonates, which may indicate not only a decrease in osteoclast activity but an increase in osteoblast activity [25]. Bisphosphonates have also been used in conjecture with other bone loss prevention treatments. One such study compared the use of bisphosphonates, HRT, and the combination of the two on their ability to prevent bone loss [24]. The use of a bisphosphonate called etidronate with and without HRT was observed over a 4 year study. Figure 10 diagrams the results of this study showing that the BMD of the spine increased by 6.8% with the use of etidronate, 6.8% with the use of HRT, and by 10.9% when etidronate and HRT were combined as treatment [24]. This suggests that the combination of multiple treatments that affect the activity of osteoclasts may be the most optimal form of treatment.

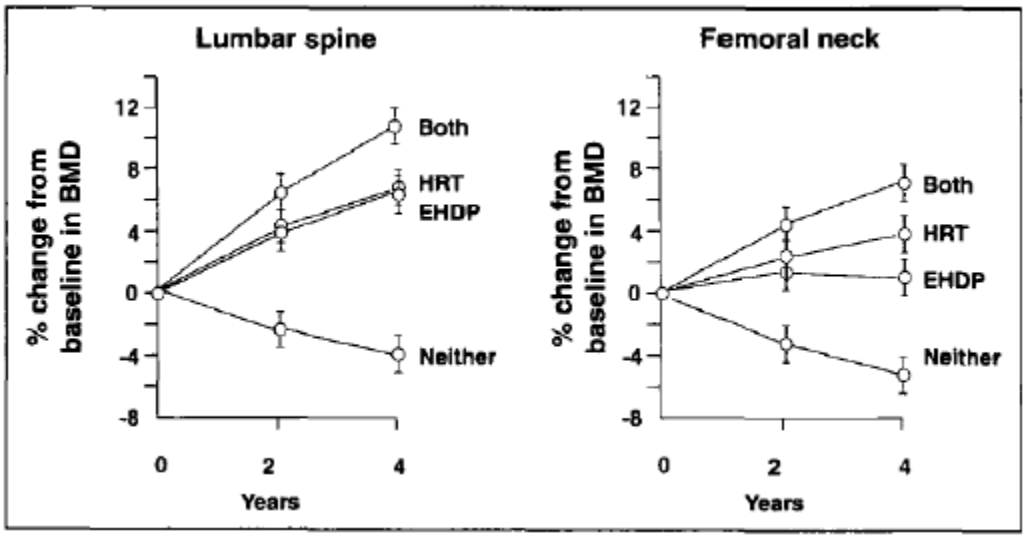

Figure 10 Lumbar spinal bone mineral density (BMD) increased similarly in estrogen and etidronate treated patients and by a greater amount using both. EHDP=etidronate; HRT=hormone replacement therapy [24]

1.5 Animal Models

The US Food and Drug Administration (FDA) have set safety and efficacy requirements that must be met before any device or pharmaceutical can be used in human treatments. To meet these standards extensive bench and animal testing (also referred to as *in vivo*) are performed. Bench and in vivo testing is used to display general proof of concept of the suggested treatment. Animal tests are the next important step in the process to be able to test potential therapies in a very complex living system. Animal tests also provide us a better means to understand how specific diseases actually affect and progress in a living system. Animal studies will typically begin with the use of small animals such as mice and rats to mitigate possible risk, allow for larger samples, and minimize the time and cost of the initial test. As a therapy proves to be safe and effective in smaller animal tests, the next step is moving onto animal testing with animals that are more physiologically relevant to humans for the proposed treatment, which tend to be

larger mammals. Although certain animal models can be very physiologically similar to humans, the need for more accurate simulations of human nutritional needs, lifestyle, and physical activity are required to fully meet FDA approval. This is the point in the testing process at which human clinical trials begin.

In the case of using animal models for treatments of osteoporosis, the animal models being involved must simulate osteoporotic conditions in order to test possible drug treatments [26]. The need for large animal models with some characteristics of human osteoporosis is especially necessary in the design of prosthetic devices with different coatings to promote osseointegration. These types of devices must be able to perform and not loosen with decreased bone mass. The use of smaller animals is impossible when testing human sized devices [26].

There are many different animals that are used for osteoporotic studies due to their varying advantages and disadvantages to the given study. Rodents, notably rats, are one of the most commonly used animals in osteoporotic studies because of the many advantages they offer. In general they are relatively inexpensive, easy to house, and are generally associated with research in the public eye. Rats also have a fairly short life span facilitating studies of the effects of aging on bone. With many studies utilizing rats, much is known about their diets effect on bone aging as well as their bone turnover [27]. It has been well documented that rat and mice models have shown cortical thinning and increased fragility of bone due to aging. Rat models, however, do not naturally go through menopause so ovariectomies are preformed to induce menopause. The rat models with artificially induced menopause effectively express similar characteristics to human postmenopausal osteoporosis making them useful in studies of the effects of

bisphosphonates on bone with estrogen deficient models [28,29]. The induced menopause rat models do, however, have a disadvantage in studying the effects of postmenopausal conditions on cortical bone because the development of Haversian canal systems and impairment of osteoblast function requires 3 to 4 months [29].

Another animal model commonly used in studies involving bone is the rabbit model. Rabbits are more commonly used in studies involving bone in growth into implants and bone implant interfaces. Very rarely are rabbit models used as an ovariectomized model to study the effects of ovarian insufficiency on bone mass [27]. The use of a rabbit model for implant models is due to rabbits undergoing Haversian remodeling, having rapid bone turnover, and showing skeletal maturity at 7 to 8 months. However, rabbits are not fully characterized for osteoporosis. Studies using a rabbit model were only able to assess BMD and not able to assess the microarchitecture and bone mechanics completely causing it to be a poor model for osteoporosis studies [30].

Dogs have been a well-used model for bone studies due to their extensive BMU remodeling and larger size. Dogs also have the advantage of being monogastric like humans and relatively easy to work with. A major difference in the physiology of dogs and humans is that dogs are diestrus, with ovulation only occurring twice a year, where humans are polyestrous and ovulate multiple times a year. This becomes a clear disadvantage for studies involving estrogen deficiency on bone. It has been shown that even with the removal of both ovaries and uteri it does not sufficiently create a significant bone loss [27]. The use of dogs in the study of postmenopausal osteoporosis is limited due to the lack of sizable response in histomorphometric, bone mass, and biochemical parameters [29].

An obvious choice of animal model to compare to humans is the use of nonhuman primates. They offer many advantages dues to their close physiological similarities including: the gastrointestinal tract, endocrine system, and bone metabolism. The two most documented species used for studies are baboons and macaques monkeys. Female macaque monkeys have a similar polyestrous cycle and hormonal patterns to humans. With an ovariectomy macaques show significant reduction in cancellous volume [29]. One major drawback is the need for the female primate to be significantly aged to act as a sufficient postmenopausal model. Other disadvantages to using primates in an animal study for osteoporosis are the high cost and difficulties of handling the animals [29].

1.5.1 Proposed Animal Model

One of the most promising animal models for osteoporosis studies is the use of skeletally mature sheep, especially the use of ewes. Sheep offer many advantages such as being of a larger size allowing for device implantation and analysis. They also offer the benefit of being easy to handle and being available in larger numbers aiding in the performance of large scale studies [31]. Sheep also offer very similar metabolic rates to humans compared to other animal models. A study showed that the metabolic rate, based on oxygen consumption per gram of body weight, in humans was .21 and sheep's metabolic rate was closest at .22 compared with that of rats (.87) and dogs (.33) [32]. Sheep also temporally and quantitatively show a similar hormone profile to those of human women [32]. Another advantage of using a sheep model is that young sheep have shown to develop plexiform bone, a combination of woven and lamellar bone. Roughly 3 to 4 months after development of plexiform bone, Haversian remodeling can be seen in the cortical bone (Figure 11) [33].

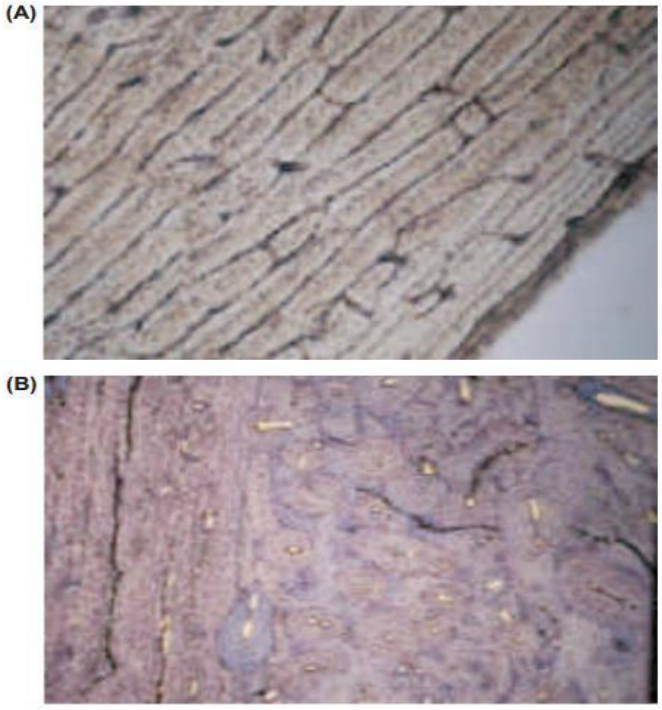

Figure 11 (A) Plexiform bone from a three-year-old ewe (original magnification x 25). (B) Haversian remodeling from the caudal femoral cortex of an eight-year-old ewe (original magnification x 25) [33]

There are, however, a few disadvantages to using a sheep model. Ewes do have a similar reproductive cycle to that of female humans, but they do not show a clear state of menopause at midlife. For this reason ewes will not be able to develop postmenopausal osteoporosis without artificially inducing menopause via ovariectomy. Ewes also go through an annual anestrous period of 1 to 2 months unlike female humans [32]. Another disadvantage of using a sheep model is their physiologically different gastrointestinal systems. In order to administer drugs orally, surgical insertion is required to bypass the microflora of the rumen, a gastrointestinal organ not found in humans [29].

Sheep that have had ovariectomies performed have been used in multiple studies of BMD loss previously. When using the ewe as the animal for a study on postmenopausal osteoporosis two major factors must be considered, the age of the animal

and the season of analysis. Older ewes have shown to be better specimens for this purpose. Research has shown that when comparing biopsies of ewes 3 months apart that there were decreases in resorption surfaces, osteoblast surface, and bone formation rates. This supports the claim that remodeling changes can occur within a 3 month period of time post ovariectomy [34]. Changes in bone mass have also been demonstrated in 3 to 4 year old ewes at the six month mark post ovariectomy (Figure 12) [34]. Other studies on osteoporosis using sheep models have shown that significant mechanical changes of the spine and ilium did not appear until 12 to 24 month post ovariectomy [35].

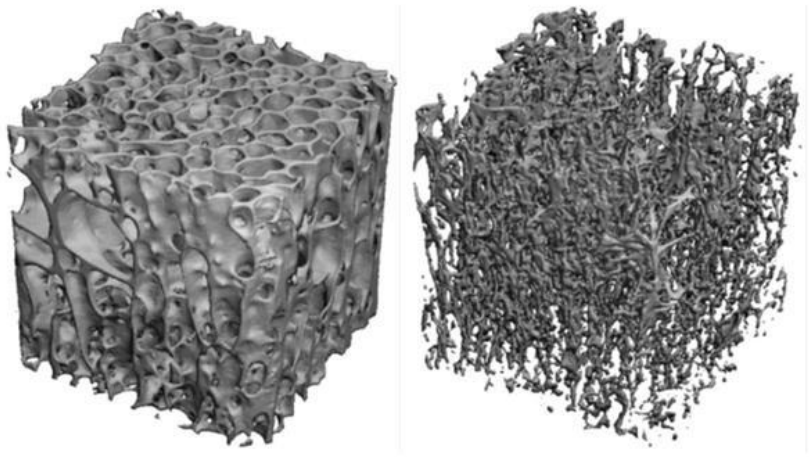

Figure 12 (Left) Three-dimensional reconstruction of a sheep vertebral body biopsy from the control group (Right) Three-dimensional reconstruction of a sheep vertebral body biopsy after 6 months of osteoporosis induction with ovariectomy, steroid application and a calcium/vitamin D-restricted diet [36]

Seasonal variation in BMD has been shown in sheep during the winter months. Humans have also been shown to have an alteration in BMD due to seasonal variation, with BMD levels being lower in the winter as well. This is thought to be caused by environmental and nutritional variation. Sheep's nutrition directly influences their bone metabolism, in particular the amount of calcium and vitamin D intake. Vitamin D is produced in the skin of animals from the exposure to ultraviolet (UV) radiation. It is then

important to consider the amount of time the animals are exposed to light and the daytime length during each season of the year [31].

The sheep model has shown to be an overall adequate model for postmenopausal osteoporosis once ovariectomized. The model will allow for testing of therapeutic agents and prosthetic devices in a very similar atmosphere as in humans. The effects of seasonality still need to be further characterized to understand their possible effects on the study. Through the following research, a quantifiable model for bone remodeling in an ovariectomized animal with further characterization of seasonal and anatomical variations will be made through comparison with control animals.

1.6 Study Objectives

The purpose of the current research project is to record empirical data concerning the histomorphometry and densitometry of a section of sheep bone samples to further understand the effects of estrogen depletion on compact bone secondary remodeling. The amount of remodeling will be assessed using the following measurements and calculations: the ratio of bone volume to tissue volume, the fraction of tissue remodeled, the fraction of material remodeled, cement line interfaces as a function of tissue volume, cement line interfaces as a function of material volume, osteons per mm^2, mean osteon area, and bone mineral density. The section of sheep the research for the project will be performed for contains the 3 month summer control sheep and OVX sheep taking measurements form the cortical bone of the radial-ulna of the ovine's left leg. Analysis will be made for variations in anatomical location and treatment.

Previous research has shown that sheep do in fact undergo seasonal variations in bone properties [31]. The research on comparing the effects of anatomical location on

remodeling parameters has been minimal and it is expected that both seasonality and anatomical location will have significant effects on remodeling parameters. In this portion of the study only 3 month summer sheep were used, so no analysis was taken to see the effects of seasonality. In this study comparisons of anatomical variation and possible variations between OVX sheep and the control sham operated sheep will be assessed for variations in remodeling parameters due to treatment. This research will further show that relevant data about postmenopausal osteoporosis will be obtained from the use of a sheep animal model.

2. Materials and Methods

2.1 Animal Maintenance and Preparation

112 skeletally mature Columbia-Rambouillet cross ewes, 5 years or older, were acquired and kept at Colorado State University, Fort Collins, Colorado as part of a larger experiment. The acquisition and housing of the animals was performed under the approval of the Animal Care and Use Committee. The animals were kept at 1500 m altitude in dry lots at 41deg north for the duration of the experiment. The animal's diet consisted of a grass-alfalfa hay mixture. The 112 ewes were separated into four groups of 28 to account for each varying season: autumn, winter, spring, and summer. Once in seasonal groups the group was further divided into two groups containing 14 ewes. The animals were then taken to the large animal surgery facilities at the College of Veterinary Medicine and Biomedical Sciences at Colorado State University, where they were anesthetized to undergo surgery. Surgeries took place during the specified group's season. The autumn, winter, spring, and summer surgeries took place in November, February, May, and August respectively. Two types of surgery where performed for the varying groups. One group of 14 from each seasonal group underwent an ovariectomy (OVX) in which the ovaries were identified and removed. The other remaining group of 14 ewes from each seasonal group would act as the control group for the experiment and underwent a sham surgery in which the ovaries were identified, handled, and not removed to make sure both OVX and control groups went under as similar stress as possible. Once the surgeries were complete the groups of 14 were again divided into two more groups of 7. One group would be sacrificed at the 3 month mark after surgery and the other group would be sacrificed at the 12 month mark after surgery. One of the 12 month autumn

sham sheep died prematurely and thus was included in the 3 month autumn data as part of another experiment. The 3 month OVX animals and 3 month control animals for the summer season were the experimental subjects for this study.

2.2 Specimen Preparation

Once the animal has been sacrificed the specimen's right and left radial-ulna were removed. The bones were then wrapped in a saline-saturated paper towel then sealed in plastic bags and kept at a temperature of -20(deg)C. The bone samples were then transported to the Henry Ford Hospital. Once delivered the samples underwent preparation for analysis. The center 50 mm of the diaphysis was removed from each sample using a ban saw (Model 5212, Hobart Corporation, Troy, OH). The section of the radius-ulna was then divided into six anatomical sectors using the Exakt cutting-grinding system (Exakt Corporation, Oklahoma City, OK). The six sectors were based on the orientation of the bone: cranial, caudal, craniolateral, craniomedial, caudomedial, and caudolateral (Figure 13).

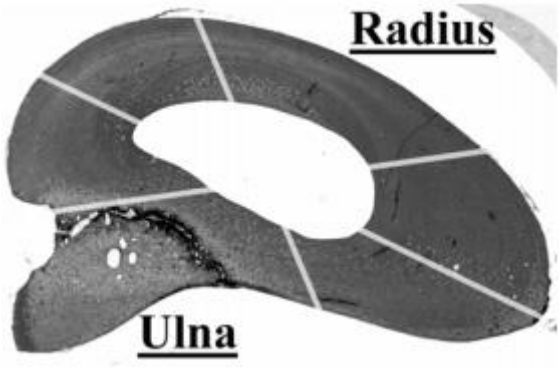

Figure 13 Approximate anatomy of the radial-ulnar sectors divided into six sections as indicated by the grey lines. The top right is the cranial aspect and the top left is the lateral aspect [37]

Longitudinal cortical beams were taken from each sector with dimensions of 1.75 x 1.75 x 19mm. In another study the cortical beams from the left radial-ulna were used in

dynamic mechanical testing. 150 μm sections were cut from the center of the left radial-ulna beams and the remaining distal ends were used for drying and ashing to provide a method to determine the samples densities. The proximal sections were frozen for analysis to be performed at a later time.

The 150 μm sections were ground down by hand to a final thickness of 100 μm using fine grit sand paper to prepare the samples to create microradiographs. Microradiographs were taken of each section using a 2506AGHD 2.5x2.5x0.06 High Definition Photo Emulsion Plates and a HP Cabinet Faxitron (HTA Enterprises, Microtome Technology Product, San Jose, CA). The images were done at 25kV for 20 minutes at 3mA. Each microradiograph consisted of the six sections of the radial-ulna of two sheep on both sides and an aluminum step wedge made with increasing layers of Reynolds Aluminum Foil in the middle (Figure 14). Aluminum foil was used as a step wedge to compare densities because it has a similar atomic number to the effective atomic number of hydroxyapatite [38]. The step wedge was created by taping increasing layers of aluminum together in a stair step pattern to create increasing levels of aluminum thicknesses in a sequential order. Each step in the step wedge is a known thickness and can be used to compare the light intensities of each step of aluminum to that of the bone samples image to create a method to measure the density of the bone sample as compared to the aluminum.

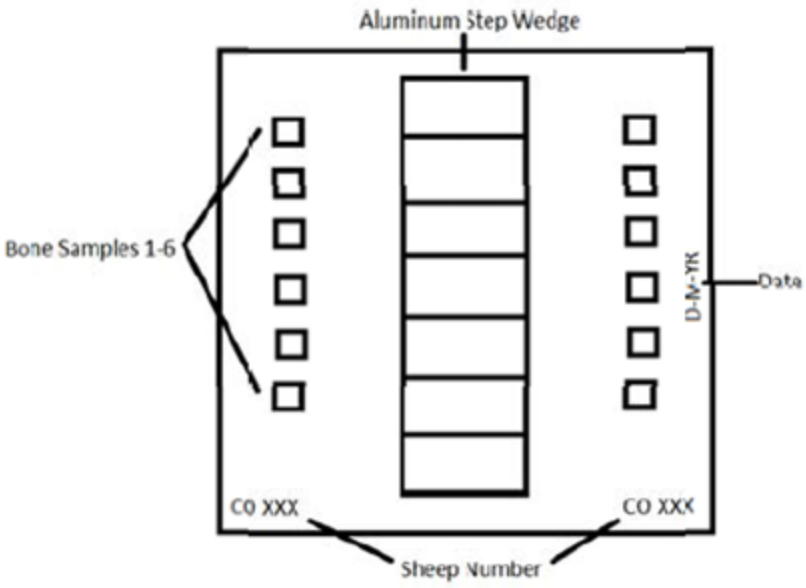

Figure 14 Diagram of microradiograph layout

2.3 Microradiograph Analysis

The microradiographs were sent from the Henry Ford Hospital to California Polytechnic State University, San Luis Obispo for analysis by students in the biomedical engineering program. The analysis conducted included histomorphometric measurements and densitometry measurements of the bone samples. The histomorphometric measurements were taken to obtain a quantifiable amount of remodeling occurring in the ovine models. These measurements included: porosity, number of secondary osteons, number of cement line interfaces, and the amount of remodeled bone. Densitometry measurements were taken to quantify the density of the bone specimens. To obtain these measurements the microradiographs were observed using an Olympus BX41 microscope (Olympus Optical Co., Ltd, Center Valley, PA) under white light at an objective of 10X.

2.4 Histomorphometry

Techniques from R.R. Recker's Text, Histomorphometry: Techniques and Interpretation were used for performing the research. [39] For this project there had already been some histomorphometry measurements taken for some of the samples. This gave a general template to follow while collecting data. This template helped organize the findings and gave something to have a loose comparison to. For the current project, a Merz grid, seen in Figure 5 previously, was used in the eyepiece of the microscope to perform the histomorphometric measurements on the 8 control and 8 OVX sheep sections used in this portion of the study. Next the stage of the microscope was modified to hold the radiographs. A slide holder was created from a sheet of acrylic by cutting it to the proper dimensions to hold the radiographs level on the microscope stage. Once the holder was finished the slides were checked to make sure they fit properly and that the holder did not interfere with the viewing.

Measurements were taken in four regions (named Northwest, Northeast, Southwest, and Southeast) for each bone sample and averaged for increased accuracy. To begin the Merz grid was oriented in the northwestern corner of the bone sample (Figure 15).

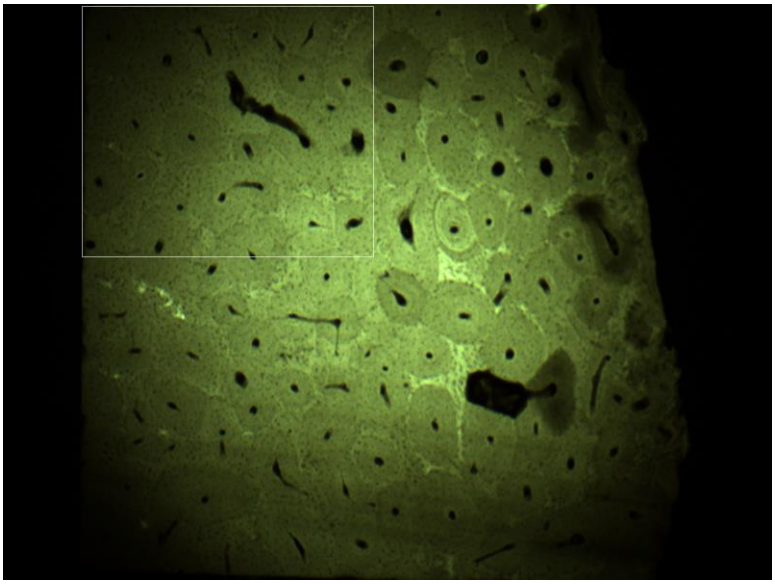

Figure 15 The white box represents northwestern corner then if you were to move the box to the right to the edge of the visible bone sample that would be considered the northeastern section. If the box is moved to the bottom right corner that would be considered the southeastern section and if placed in the lower left would be considered the southwestern region.

Once the slide was focused the Merz grid was used to count the number of pores (called porosity or void space) that intersected with the dashes on the Merz grid (Figure 5). Porosity was considered any space which was visibly “black” (porous) which would typically occur from Haversian canals, Volkman's canals, or remodeling cavities on the slide (Figure 16).

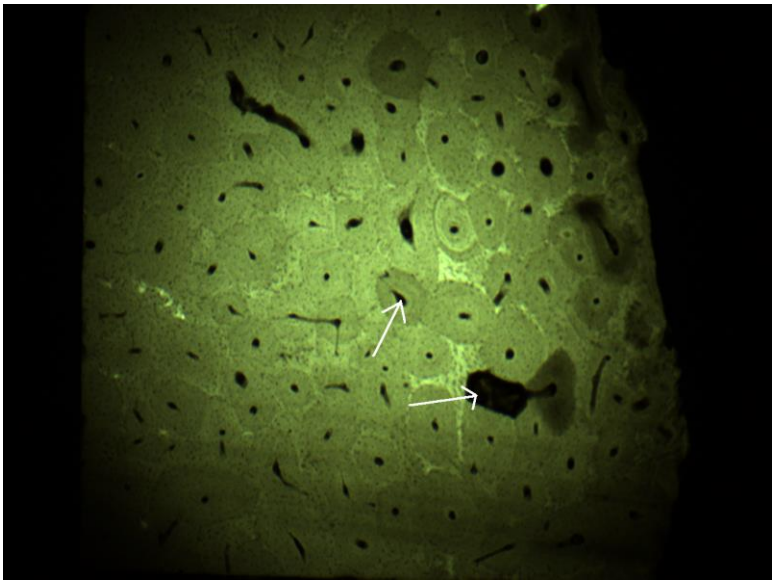

Figure 16 White arrows point to areas considered “Porous”

The data would then be recorded. To quantify the amount of remodeled bone the dashes on the Merz grid that intersected with the “new remodeled bone” were counted with a hand tally counter. Once counted the data was recorded in the corresponding table. New remodeled bone would be any area of bone within the area contained by a cement line interface (an area that clearly had a new cement line around an osteon) (Figure 17).

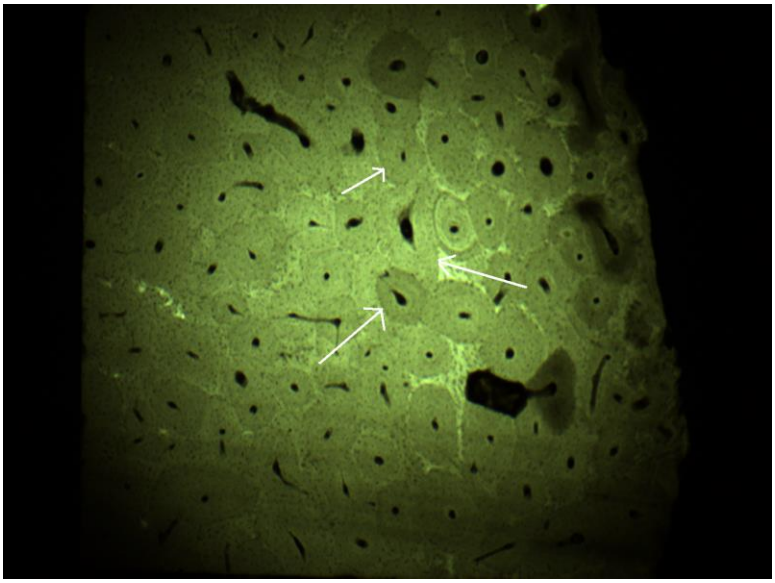

Figure 17 White arrows point to the cement line interface (the area where the color changes)

The next step was to point count the number of osteons (primary and secondary) per field. This was done by counting the osteons within the Merz grid only and record the number found. Secondary osteons were characterized by their prominent features which include their circular nature, centering on a Haversion canal, the circular patterns by osteocyte lacunae, and surrounding cement line. To minimize repeat counts, osteons along the upper and right border of the grid would be counted and osteons along the lower and left border would not be counted. The last histomorphic measurement to be taken was the cement line interfaces. This was obtained by counting the number of times the Merz grid's "waves" (Figure 5) would cross a cement line interface. Once these four measurements were completed and recorded the Merz grid would be moved to be oriented in the northeast corner and the above steps would be repeated. The grid would then be moved to the southeast section and finally to the southwest corner repeating the steps again. Once all of the point counting was completed for a section of bone the data would be recorded into an excel chart. It should also be noted that some bone samples were damaged or missing, these areas were omitted from taking data as there was not a significant amount of bone to take measurements from. The averages and standard deviations were calculated using excel for the four different locations for each specimen. The previous methods would then be repeated for all of the 3 month summer slides and all the data would be recorded in the excel sheet 3moSummer-RAWdata. Once all the data was collected the averages of the previously calculated averages for the four regions per specimen were calculated for each OVX (ovariectomy sheep) and control sheep to see if there was any visible correlation between them.

Once all of the raw data was collected it was then used to compute the bone

volume fraction (BV/TV), fraction of tissue remodeled, fraction of material remodeled, osteons per mm^2, osteons per mm^2 of material, osteons per mm^2 of remodeled material, mean osteon area, the cement line interface for tissue, the cement line interface of material, and the cement line interface of remodeled material, this data was recorded in an excel spreadsheet. These were calculated with the equations below (equations 2,3,4,5,6,7,8,9) . In the equations used the 36 refers to the number of intersection points on the Merz grid.

$$BV/TV = (1-(Porosities)/36)) \quad (Eq.\ 2)$$

$$Fraction\ of\ Tissue\ Remodeled = (Remodel/36) \quad (Eq.\ 3)$$

$$Fraction\ of\ Material\ Remodeled = (Remodel)/\ (36-Porosities) \quad (Eq.\ 4)$$

$$Osteons\ per\ mm^2\ (1/mm^2) = (Osteons/x^2) \quad (Eq.\ 5)$$

$$Osteons\ per\ mm^2\ (Material)(1/mm^2) = (Osteons/x^2)/(Eq.\ 2) \quad (Eq.\ 6)$$

$$Osteons\ per\ mm^2\ (Remodeled\ Material)\ (1/mm^2) = (Osteons/x^2)/(Eq.\ 4) \quad (Eq.\ 7)$$

$$Mean\ Osteonal\ Area\ (\mu m\text{^}2) = 1/((Eq.7)((x)*10^6) \quad (Eq.\ 8)$$

$$CLI/mm^2\ of\ Tissue = ((\#\ of\ CLI)(4.752))/(6*x) \quad (Eq.\ 7)$$

$$CLI/mm^2\ of\ Material = (((\#of\ CLI)/(\ Eq.2))(4.752))/(6*x) \quad (Eq.\ 8)$$

$$CLI/mm^2\ of\ Remodeled\ Material = (Eq.3)/(Eq.8) \quad (Eq.9)$$

To further explain the reasons behind using the above equations first the BV/TV equation indicates the amount of porosity in the sample by dividing the recorded porosity of the sample by the max amount of porosity (36, the number of dashes on the Merz grid) and subtracting that value from one. This then gives us a ratio of porosity compared to the amount of bone observed. The next two equations represent the amount of tissue that was remodeled (fraction of tissue remodeled) by dividing the number of remodeled bone

observed in the section by 36 to find the fraction of remodeled tissue. The amount of bone remodeled (fraction of material remodeled) was the observed remodeled bone divided by 36 minus the observed porosities to obtain only the fraction of remodeled bone. The Osteon/ Field equation indicates amount of osteons found within the field. Field is defined by the visible area (mm^2) within the Merz grid used in the optics of the microscope. Specifically x in equation 5 represents the length of the sides of the Merz grid seen at 10X magnification. The Merz grid used had a dimension of 1mm x 1mm at 10X magnification, found using a micrometer. X then equaled 1mm in this study. The Osteon/Field (Material) equation explains the density of osteons in material as compared to tissue, where if BV/TV =1.00, then Material = Tissue. If BV/TV < 1, then the osteonal density per area of material is higher than is the osteonal density per area of tissue. The Osteon/Field (Remodeled Material) explains the density of osteons in remodeled material as compared to material in the same way as Osteon/Field (Material) using the Fraction of Remodeled Material instead of BV/TV. The Equation for Mean Osteonal Area is calculated by taking 1 over the amount of Osteons/mm^2 (Eq. 7) multiplied by 10^6 to convert to microns. This gives the Mean Area of an osteon in the observed field. The equations for CLI/mm^2 were found using the CLI recorded multipled by ((4.752)/(6x), found by using equations in R.R. Recker's Text, Histomorphometry: Techniques and Interpretation for the Merz grid [39].

2.5 Densitometry

For the next portion of research pictures were taken of the slides under the Olympus BX41 polarizing light microscope using a Retiga Exi color camera (QImaging, Surrey, BC, Canada) along with Q Capture Pro imaging prgram (QImaging). Pictures

were taken of each sample in 4 quadrants (Northwestern, Northeastern, Southeastern, Southwestern) at 10x magnification and a picture of each of the steps located on the step ladder (1-6 including one for closed shutter and one for the black background of the radiograph) of each of the slides used (Figure 18).

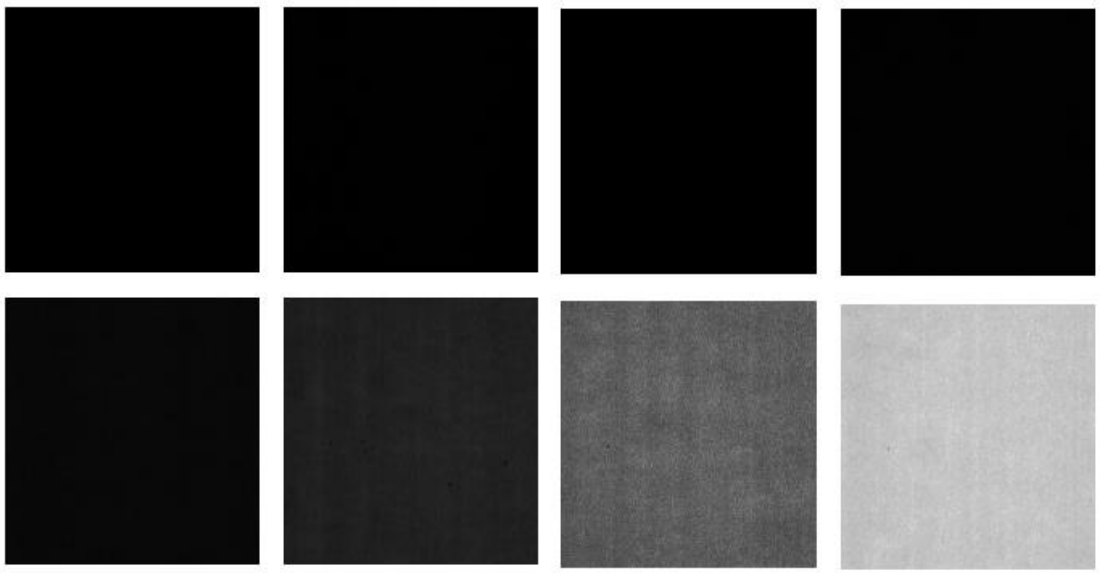

Figure 18 Sample of ladder from slide C14C15 used in density calculations, from left to right top to bottom (Shutter closed, black background of radiograph = 0mm, Level 1 = 0.02mm, Level 2 = 0.04mm, Level 3 = 0.06mm, Level 4 = 0.08mm, Level 5 = 0.1mm, and Level 6 = 0.12mm respectively)

The step wedge of the slides was created using increasing layers of aluminum foil to be used as the reference material to quantify the bone density of the samples. Aluminum is commonly used due to it having similar x-ray attenuation as that of cortical bone [38, 40]. Knowing the thickness of the aluminum we could describe the measurements of density as the equivalent thickness of aluminum (ETA) measured in millimeters. Images were taken of the bone samples and corresponding step ladders under the same conditions: optimal light intensity, time of day, and surrounding light sources.

Once the images were obtained, image analysis was performed using the software

Image J (Wayne Rashband (NIH)). The density and thickness of the material corresponds directly to the lightness and brightness of the images, whereas the brightness and lightness increases so does the thickness and density of the material. This can be seen in the example of the step wedge above (Figure 18). Each step in the step wedge corresponds with a known thickness. One sheet equaling 0.02mm and each step increasing by one sheet, ranging from 0 – 6 sheets which is equal to 0.00mm – 0.12mm respectively. Using Image J, histograms of the pixel intensity of the images were found. The pixel range was from 0-255, 0 being black and 255 being white. These histograms were then recorded and mean pixel intensities were determined for each level of the step wedge. Using the mean pixel intensities of each step of the step wedge and the known thicknesses of the steps the 4-parameter sigmoid curve (equation 10) could be found using SigmaPlot 12.3 (Systat Software, Inc.). Where Y = y-axes intercept, Y_o= initial Y intercept, x = x-axis intercept, x_o= initial x intercept, a = MAX asymptote, b = minimum asymptote. The 4-parameter sigmoid curve could then be used as the calibration parameters necessary for determining the ETA of each bone sample.

$$Y = Y_o + a / (1 + e^{-(x-xo/b)}) \qquad \textit{(Eq. 10)}$$

The next step was to analyze the samples. Using Image J, a similar process was used to measure the brightness of the images finding the pixel intensity of the samples. The pixel intensity of each quadrant of a sample was found and using the calibration parameters the pixel intensity values could be converted to ETA. These measurements were performed for all samples and their corresponding step wedges. These measurements accounted for porosity by taking all of the counted porosity found during the raw data collection for each sample and dividing that number by 144, the total

number of possible points. This value represented the proportion of pixels that represent non-bone in the images, Q. Using this value data was deleted until the remaining pixels equaled 1 minus Q, starting with the lowest ETA pixels.

2.6 Statistical Analysis

Once the data was collected statistical analysis was performed using a 2-way Repeated Measures ANOVA test in SigmaPlot 12.1 (Systat Software, Inc.). This test was chosen to be able to measure the differences between treatment, anatomical sector, and calculated measurements (BV/TV, fraction of remodeled material, fraction of remodeled tissue, osteons per mm^2 (material, osteons per mm^2 (remodeled material), mean osteon area, CLI (bone), CLI (tissue), and CLI (remodeled material)). To make comparisons with the analysis, the *post-hoc* Fisher Least Significant Difference (LSD) test was used with a significance level of 0.05 used. The Least Significant Difference method is to first test the null hypothesis that all the population means are equal (the omnibus null hypothesis) with an analysis of variance. If the analysis of variance is not significant, then neither the omnibus null hypothesis nor any other null hypothesis about differences among means can be rejected. If the analysis of variance is significant, then each mean is compared with each other using a t-test. The results of the test were then reviewed to see if the sectors or treatment did have a significant difference from their comparables. A 2-way Repeated Measures ANOVA test was also used for statistical analysis of the ETA of the bone samples to analyze if there was a difference seen between treatment, anatomical sector, and the combination of both test and sector.

3. Results

3.1 Histomorphometry

Histomorphometric measurements were taken for Summer 3 month OVX and Control sheep. For each of the six sectors, the average value calculated from the four quadrants of the samples were found for BV/TV, the fraction of remodeled tissue, the fraction of the remodeled material, osteons/mm^2 for material, osteons/mm2 for remodeled material, mean osteonal area, cement line interfaces of the tissue, and the cement line interfaces of the material, cement line interfaces of the remodeled material. The averages and standard deviations for each test and anatomical sectors are found in Tables I - IX.

Table I Bone volume to tissue volume for adult 3 month summer OVX and Control ovine compact bone

BV/TV(OVX)		
Anatomical Sector		
Group	Mean	Standard Deviation
Craniomedial	0.956	0.027
Cranial	0.967	0.030
Craniolateral	0.952	0.038
Caudomedial	0.948	0.024
Caudal	0.956	0.037
Caudolateral	0.961	0.022
BV/TV(Control)		
Anatomical Sector		
Group	Mean	Standard Deviation
Craniomedial	0.964	0.024
Cranial	0.966	0.032
Craniolateral	0.967	0.026
Caudomedial	0.969	0.023
Caudal	0.937	0.039

Table II Fraction Remodeled Tissue for adult 3 month summer OVX and Control ovine compact bone

Fraction Remodeled(Tissue) (OVX)		
Anatomical Sector		
Group	Mean	Standard Deviation
Craniomedial	0.440	0.062
Cranial	0.434	0.062
Craniolateral	0.489	0.069
Caudomedial	0.461	0.081
Caudal	0.493	0.057
Caudolateral	0.427	0.062
Fraction Remodeled(Tissue) (Control)		
Anatomical Sector		
Group	Mean	Standard Deviation
Craniomedial	0.386	0.054
Cranial	0.416	0.055
Craniolateral	0.461	0.070
Caudomedial	0.477	0.071
Caudal	0.568	0.080
Caudolateral	0.344	0.051

Table III Fraction Remodeled Material for adult 3 month summer OVX and Control ovine compact bone

Fraction Remodeled(Material) (OVX)		
Anatomical Sector		
Group	Mean	Standard Deviation
Craniomedial	0.461	0.062
Cranial	0.449	0.059
Craniolateral	0.513	0.071
Caudomedial	0.485	0.081
Caudal	0.516	0.058
Caudolateral	0.444	0.059
Fraction Remodeled(Material) (Control)		
Anatomical Sector		
Group	Mean	Standard Deviation
Craniomedial	0.401	0.055
Cranial	0.431	0.053
Craniolateral	0.477	0.072
Caudomedial	0.493	0.071
Caudal	0.608	0.077
Caudolateral	0.354	0.051

Table IV Osteon Per mm^2 ($1/mm^2$) (Material) for adult 3 month summer OVX and Control ovine compact bone

Osteon Per mm^2 (Material) ($1/mm^2$)(OVX)		
Anatomical Sector		
Group	Mean	Standard Deviation
Craniomedial	39.4	7.39
Cranial	32.0	6.17
Craniolateral	30.2	5.52
Caudomedial	33.5	8.05
Caudal	33.5	6.22
Caudolateral	33.5	7.86
Osteon Per mm^2 (Material) ($1/mm^2$)(Control)		
Anatomical Sector		
Group	Mean	Standard Deviation
Craniomedial	42.2	6.37
Cranial	30.3	9.74
Craniolateral	35.3	6.44
Caudomedial	34.9	8.08
Caudal	31.9	6.20
Caudolateral	31.4	8.29

Table V Osteon Per mm^2 ($1/mm^2$) (Remodeled Material) for adult 3 month summer OVX and Control ovine compact bone

Osteon Per mm^2 (Remodeled Material) ($1/mm^2$)(OVX)		
Anatomical Sector		
Group	Mean	Standard Deviation
Craniomedial	90.2	20.7
Cranial	73.3	16.8
Craniolateral	61.5	11.9
Caudomedial	74.9	29.6
Caudal	67.2	13.2
Caudolateral	83.4	23.5
Osteon Per mm^2 (Remodeled Material) ($1/mm^2$)(Control)		
Anatomical Sector		
Group	Mean	Standard Deviation
Craniomedial	111	25.2
Cranial	73.3	28.9
Craniolateral	75.6	15.2
Caudomedial	75.3	23.8
Caudal	54.9	17.2
Caudolateral	129	134

Table VI Mean Osteonal Area (μm^2) for adult 3 month summer OVX and Control ovine compact bone

Mean Osteonal Area (μm^2)(OVX)		
Anatomical Sector		
Group	Mean	Standard Deviation
Craniomedial	12100	2500
Cranial	14500	3180
Craniolateral	17200	3090
Caudomedial	15600	5980
Caudal	16100	3550
Caudolateral	13400	3440
Mean Osteonal Area (μm^2)(Control)		
Anatomical Sector		
Group	Mean	Standard Deviation
Craniomedial	10100	3470
Cranial	15200	4100
Craniolateral	14000	3060
Caudomedial	15000	4250
Caudal	19900	4870
Caudolateral	11700	4050

Table VII Cement line interfaces (Tissue) for adult 3 month summer OVX and Control ovine compact bone

Cement Line Interfaces (Tissue) (mm/mm^2)(OVX)		
Anatomical Sector		
Group	Mean	Standard Deviation
Craniomedial	42.3	6.82
Cranial	38.5	6.59
Craniolateral	40.7	9.37
Caudomedial	41.9	9.03
Caudal	44.1	6.21
Caudolateral	38.1	7.04
Cement Line Interfaces (Tissue) (mm/mm^2)(Control)		
Anatomical Sector		
Group	Mean	Standard Deviation
Craniomedial	37.7	3.92
Cranial	36.0	6.35
Craniolateral	42.1	7.69
Caudomedial	44.9	8.77
Caudal	46.8	7.03
Caudolateral	31.2	12.9

Table VIII Cement line interfaces (Material) for adult 3 month summer OVX and Control ovine compact bone

Cement Line Interfaces (Material) (mm/mm^2)(OVX)		
Anatomical Sector		
Group	Mean	Standard Deviation
Craniomedial	44.3	7.31
Cranial	39.9	6.91
Craniolateral	42.7	9.46
Caudomedial	42.9	9.48
Caudal	46.2	6.56
Caudolateral	39.5	6.89
Cement Line Interfaces (Material) (mm/mm^2)(Control)		
Anatomical Sector		
Group	Mean	Standard Deviation
Craniomedial	39.2	4.50
Cranial	37.3	6.38
Craniolateral	43.6	8.06
Caudomedial	46.4	8.84
Caudal	50.0	6.80
Caudolateral	32.1	13.2

Table IX Cement line interfaces (Remodeled Material) for adult 3 month summer OVX and Control ovine compact bone

Cement Line Interfaces (Remodeled Material) (mm/mm^2)(OVX)		
Anatomical Sector		
Group	Mean	Standard Deviation
Craniomedial	99.0	13.2
Cranial	89.8	11.4
Craniolateral	85.4	13.8
Caudomedial	91.6	19.4
Caudal	92.0	13.2
Caudolateral	96.2	12.4
Cement Line Interfaces (Remodeled Material) (mm/mm^2)(Control)		
Anatomical Sector		
Group	Mean	Standard Deviation
Craniomedial	101	15.4
Cranial	87.4	9.8
Craniolateral	92.6	16.7
Caudomedial	95.9	12.9
Caudal	84.2	15.4
Caudolateral	99.6	27.8

3.1.1 Two Way Repeated Measures ANOVA

A 2-way repeated measures ANOVA was performed to statistically test the OVX sheep against the control sheep, anatomical sectors against each other, and the possible variance between OVX sectors and control sectors. A p-value of less than 0.05 was considered as showing significant difference. Table X is a summary of the p-values obtained from the 2-way repeated measures ANOVA for each of the calculated remodeling parameters in this study.

Table X P – values for 2-way repeated measures ANOVA of remodeling parameters

2-way repeated measures ANOVA of remodeling parameters			
Parameter	Treatment	Sector	Interaction of Treatment and Sector
BV/TV	0.451	0.498	0.547
Fraction Remodeled (Tissue)	0.578	<0.001	0.114
Fraction Remodeled (Material)	0.562	<0.001	0.050
Cement Line Interface (Tissue)	0.622	<0.001	0.258
Cement Line Interface (Material)	0.588	<0.001	0.186
Cement Line Interface (Remodeled Material)	0.881	0.061	0.627
Osteons/mm^2 (Material)	0.750	<0.001	0.542
Osteons/mm^2 (Remodeled Material)	0.226	0.018	0.400
Mean Osteonal Area	0.581	<0.001	0.064

There was a significant variation seen between anatomical sectors in each parameter other than BV/TV, Cement Line Interface (Remodeled Material), and Osteons/mm^2 (Remodeled Material). Parameters that showed no demonstrable difference were related to Remodeled Material, specifically to the Cement Line Interfaces and Osteons/mm^2.

There was no significant variation found between OVX vs. control sheep seen in the 3 month summer sheep. There was however a significant variation when comparing

anatomical sectors between OVX and control sheep for Fraction Remodeled (Material) sector 5, Mean Osteons Area Sector 5, and Osteon Per Field (Remodeled Material) Sector 6 (Figure 21, 22, 24). The control sheep showed a higher fraction of remodeling than the OVX sheep in sector 5. Control sheep showed having a larger mean osteonal area than OVX sheep in sector 5 (Figure 22). Sector 5 refers to the caudal region of the bone. Control sheep also showed an increased mean of osteons per mm^2 (Remodeled Material) than OVX sheep in sector 6.

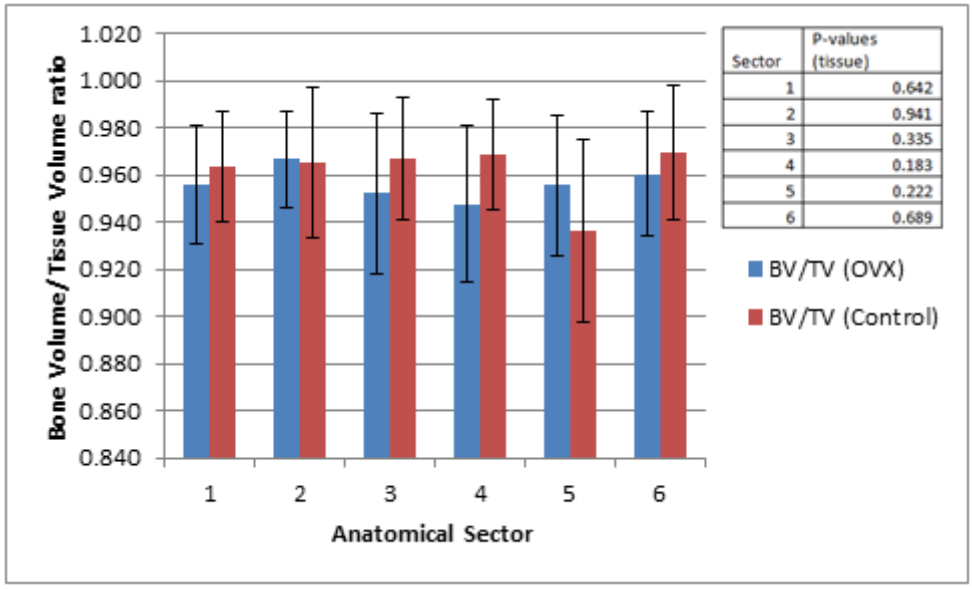

Figure 19 Mean BV/TV for control and OVX sheep for each anatomical sector.

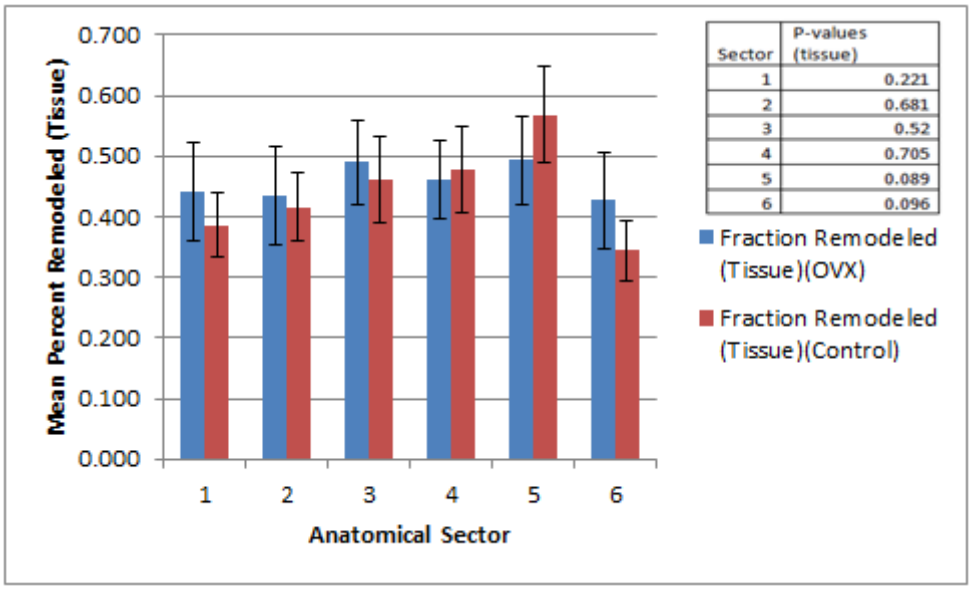

Sector	P-values (tissue)
1	0.221
2	0.681
3	0.52
4	0.705
5	0.089
6	0.096

Figure 20 Mean Fraction Remodeled (Tissue) for control and OVX sheep for each anatomical sector.

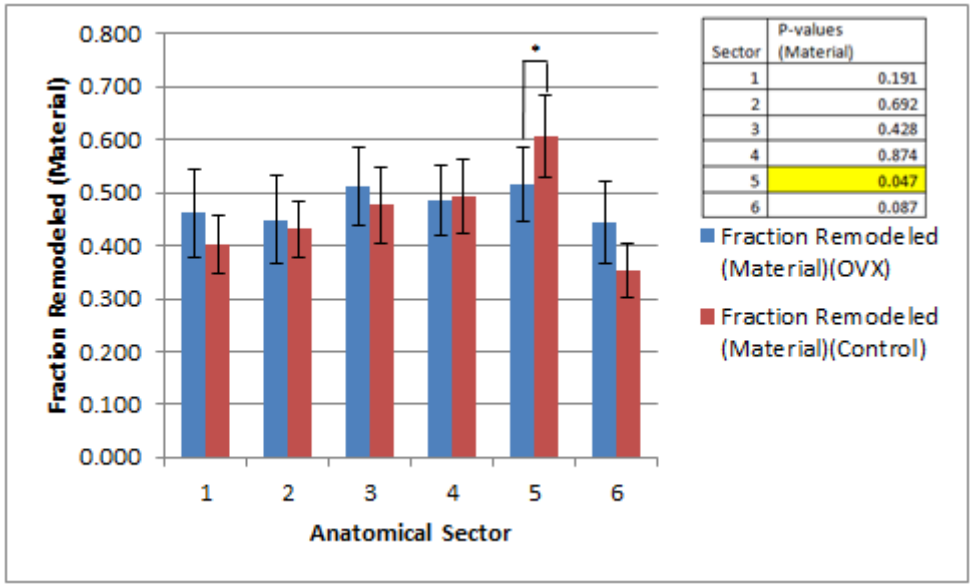

Sector	P-values (Material)
1	0.191
2	0.692
3	0.428
4	0.874
5	0.047
6	0.087

Figure 21 Mean Fraction Remodeled (Material) for control and OVX sheep for each anatomical sector. The asterisk (*) represents a significant difference.

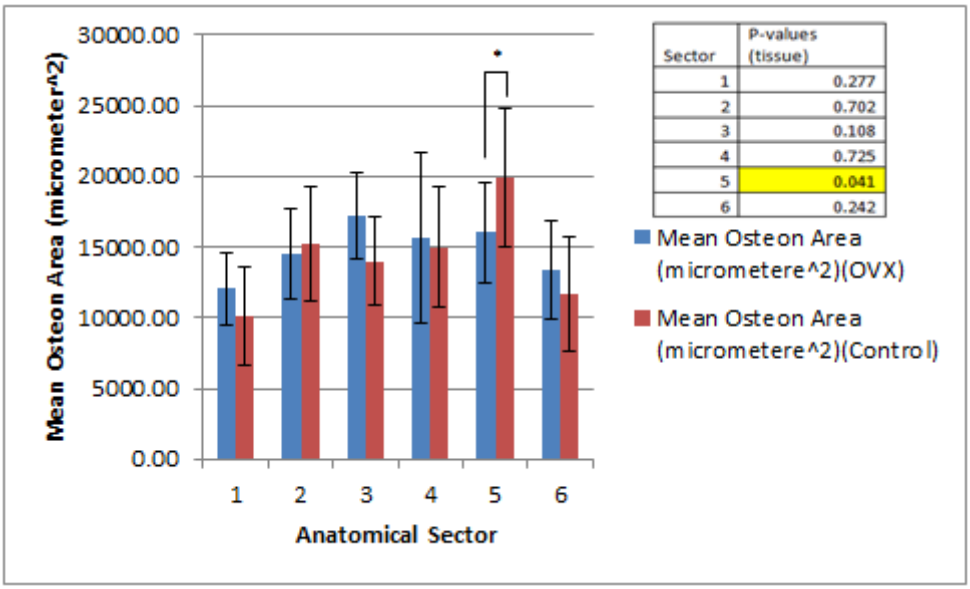

Sector	P-values (tissue)
1	0.277
2	0.702
3	0.108
4	0.725
5	0.041
6	0.242

Figure 22 Mean Osteon Area for control and OVX sheep for each Anatomical sector. The asterisk (*) represents a significant difference.

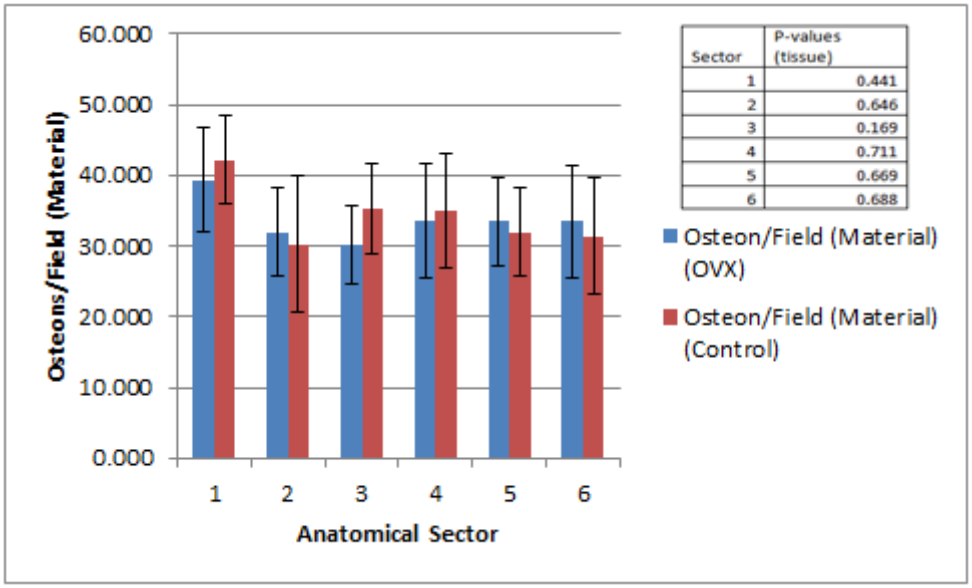

Sector	P-values (tissue)
1	0.441
2	0.646
3	0.169
4	0.711
5	0.669
6	0.688

Figure 23 Average number of Osteons Per mm^2 (Material) for control and OVX sheep for each anatomical sector.

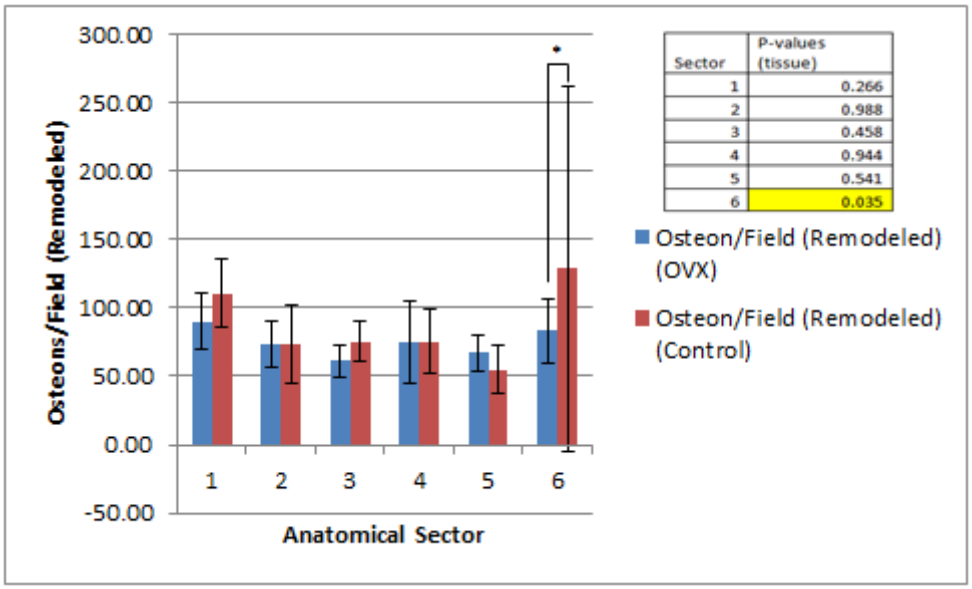

Figure 24 Average number of Osteons Per mm^2 (Remodeled Material) for control and OVX sheep for each anatomical sector. The asterisk (*) represents a significant difference.

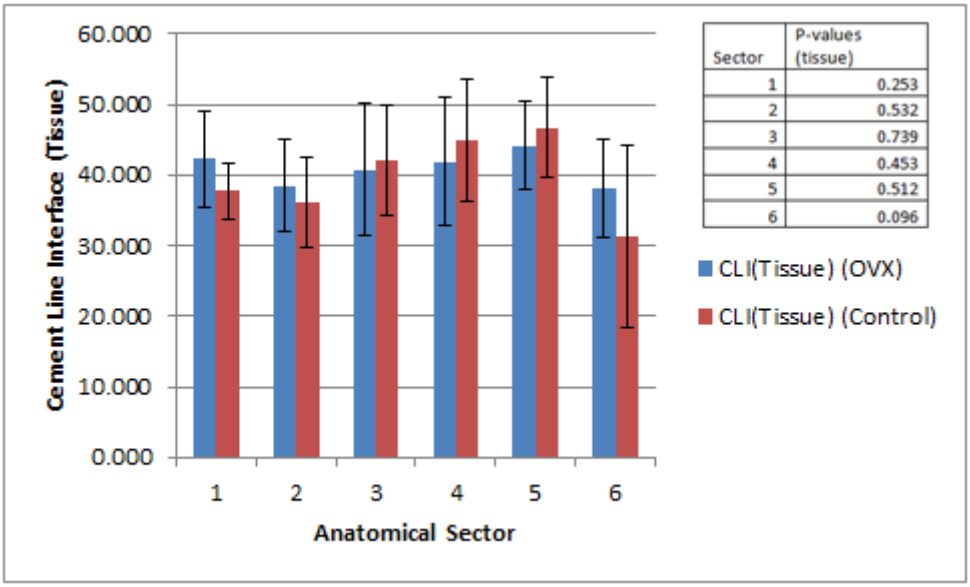

Figure 25 Average Cement Line Interface of mm/mm^2 (Tissue) for control and OVX sheep for each anatomical sector.

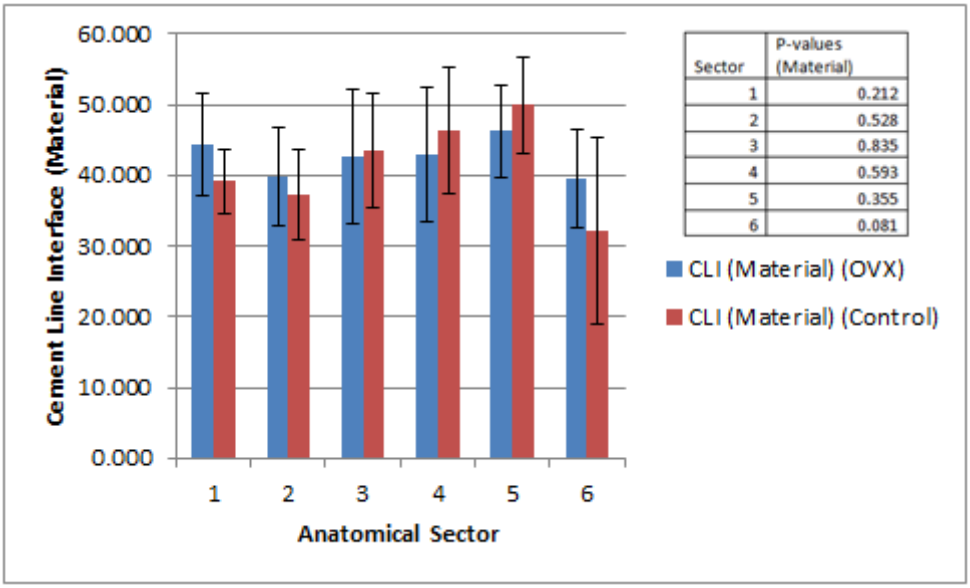

Sector	P-values (Material)
1	0.212
2	0.528
3	0.835
4	0.593
5	0.355
6	0.081

Figure 26 Average Cement Line Interface of mm/mm^2 (Material) for control and OVX sheep for each anatomical sector.

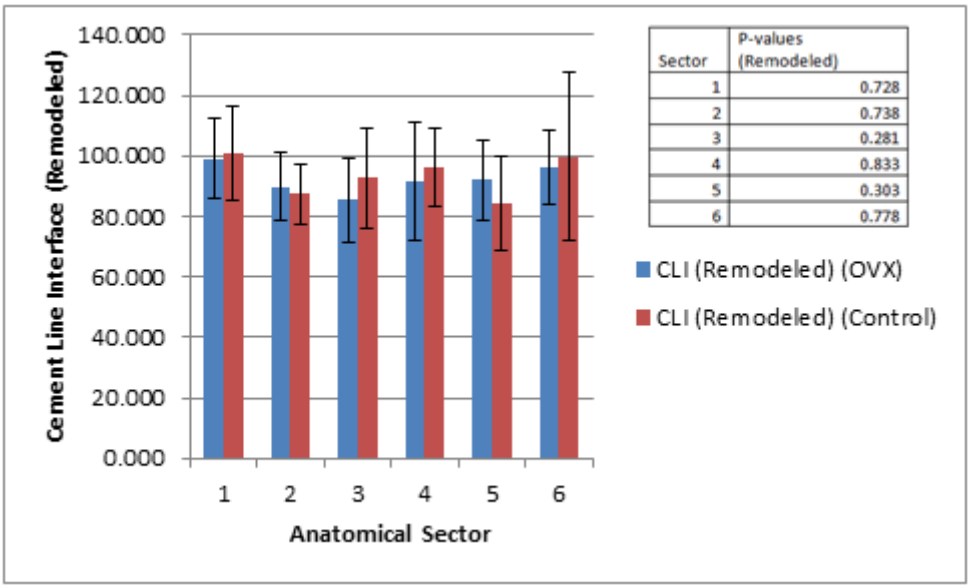

Sector	P-values (Remodeled)
1	0.728
2	0.738
3	0.281
4	0.833
5	0.303
6	0.778

Figure 27 Average Cement Line Interface of mm/mm^2 (Remodeled) for control and OVX sheep for each anatomical sector.

3.2 Densitometry

Images were taken of the bone samples and corresponding aluminum step wedges. The mean pixel intensity values of each step wedge were then determined. The mean pixel intensity values along with the known equivalent thickness of aluminum (ETA) values for the step wedges were graphed and fit to a 4-parameter sigmoid curve to create the calibration curve for each step wedge. Using the images of the bone samples, mean pixel intensities were determined for each quadrant of the sample and using the calibration curve the ETA for each quadrant was found. Measurements were taken for each sector of all 3 month summer OVX sheep and all 3 month summer Control sheep. The mean ETA values and standard error for each anatomical sector for both OVX and Control sheep is shown in Table XIV.

Table XI Mean ETA values and Standard Error of each sector in Control and OVX sheep

Average ETA's and Standard Deviations of Control and OVX Sheep		
OVX Sheep		
Sector	Average ETA	Standard Deviation
1	0.079	0.012
2	0.076	0.016
3	0.078	0.014
4	0.072	0.017
5	0.073	0.010
6	0.071	0.013
Control Sheep		
1	0.097	0.028
2	0.091	0.032
3	0.092	0.032
4	0.093	0.032
5	0.090	0.032
6	0.101	0.031

A 2-way repeated measures ANOVA was performed to statistically test the OVX sheep against the control sheep, anatomical sectors against each other, and the possible variance between OVX sectors and control sectors. Table XV is a summary of p-values obtained from the 2-way repeated measures ANOVA for ETA.

Table XII P – values for 2-way repeated measures ANOVA of ETA

P-values from 2-way repeated measures ANOVA of ETA		
Treatment	Sector	Treatment and Sector
<0.001	0.979	0.941

A statistical difference was seen in the density of the bone between the OVX vs Control sheep (Figure 28, 29). The control sheep showed a greater density in all anatomical sectors vs the OVX sheep. The greatest variance was seen between the caudolateral sectors of the two types of sheep. There was no statistical difference seen between sectors for both test groups.

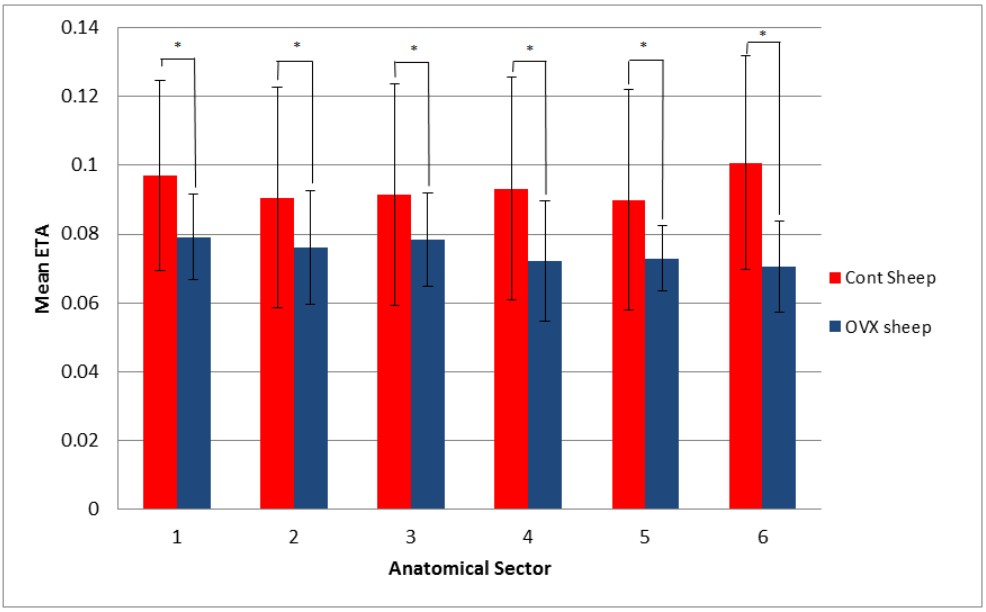

Figure 28 Average ETA of each anatomical sector of OVX vs. Control with Standard Deviation bars

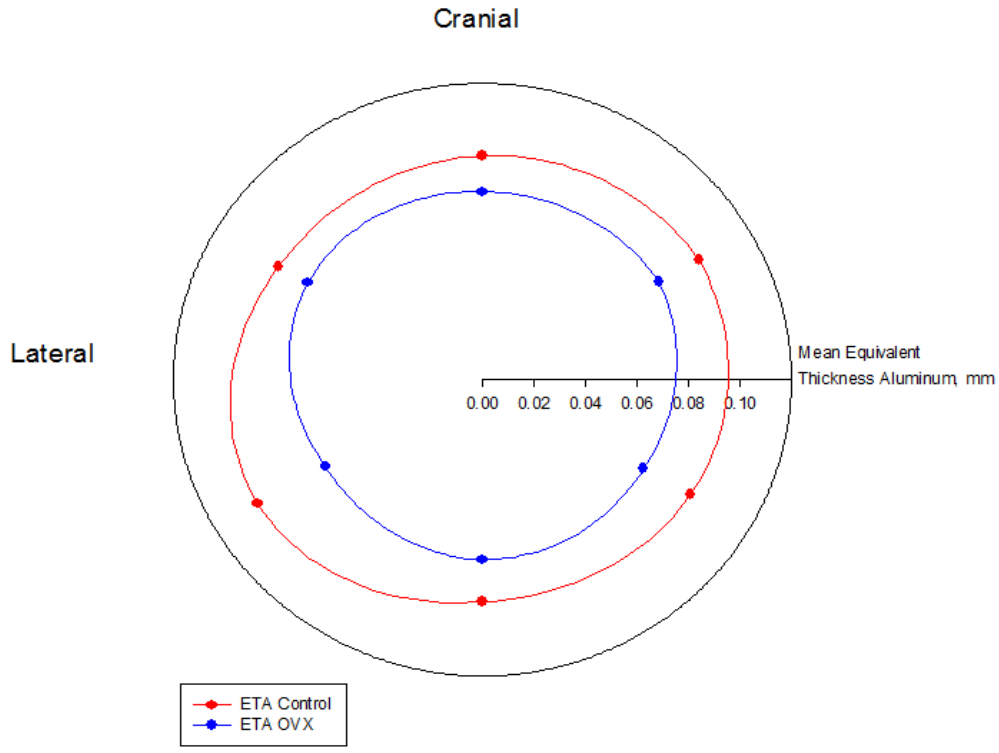

Figure 29 Anatomic variability in density measured in equivalent thickness of aluminum (ETA) for OVX and Control Sheep. The polar graph orients the values for each sector in their approximate anatomical location. The radial distance is directly proportional to the value of ETA in mm.

4. Discussion

Osteoporosis has become a universal health issue affecting millions of people [41]. With increasing age bone becomes more porous and decreases in density leading to the bone disease known as osteoporosis. Those suffering from osteoporosis are at much higher risk of bone fractures, limiting their ability to care for themselves. Currently the initial clinical manifestations of osteoporosis are due to the incidence of low-trauma fractures from such things as: coughing, rolling over in bed, or even bending over to put on shoes [41]. Patients suffering from osteoporosis experience a severe decrease in quality of life and increase their dependency on aid from others as well as other device aids to help with movement and normal tasks [42]. With an increasing population of people over the age of 50 it is imperative to improve detection methods of osteoporosis to limit the risk of bone fracture. Some methods of detecting important factors such as one's bone mineral density (BMD) exist, such as DEXA. However, most patients that are diagnosed with osteoporosis are not diagnosed until after their first low trauma fracture due to inadequate detection and diagnosis of these patients prior to the incident [43]. Many times it is difficult to correlate a trauma event with osteoporosis because the fracture can occur during a low trauma event or during a moderate trauma event [43]. To better assess if a patient is more likely suffering from osteoporosis is to first better understand the risk factors that can be associated with increased risk of osteoporosis. Some of the most prevalent risks are gender and increased age, were women are four times more likely to be affected by osteoporosis than men and the increasing risk after the age of 50 in both men and women [41]. Some other risks associated with increased chances to be affected by osteoporosis are caused by smoking, excessive alcohol and

caffeine consumption, sedentary lifestyle, and low body weight (<127 lbs) [41].

Along with understanding risk factors that lead to osteoporosis, it is also necessary to have sufficient osteoporosis detection methods to help assess a patient's likelihood of having osteoporosis. As mentioned above one commonly used method for determining the BMD is the use of DEXA. However, BMD is just one factor of assessing bone strength. The overall strength of bone and its possible fragility are influenced by multiple parameters including mineralization, bone turnover rate, and trabecular and cortical bone microarchitecture [44]. There are other methods that can further assess the microarchitecture of bone. Some of the more optimal methods include computed tomography and magnetic resonance primarily because they can assess the bone's microarchitecture in vivo. Another promising method used is high-resolution peripheral quantitative computed tomography, which can assess both bone density and its microarchitecture. Figure 30 shows that this method can allow physicians to be better able to assess a patient's osteoporotic risk.

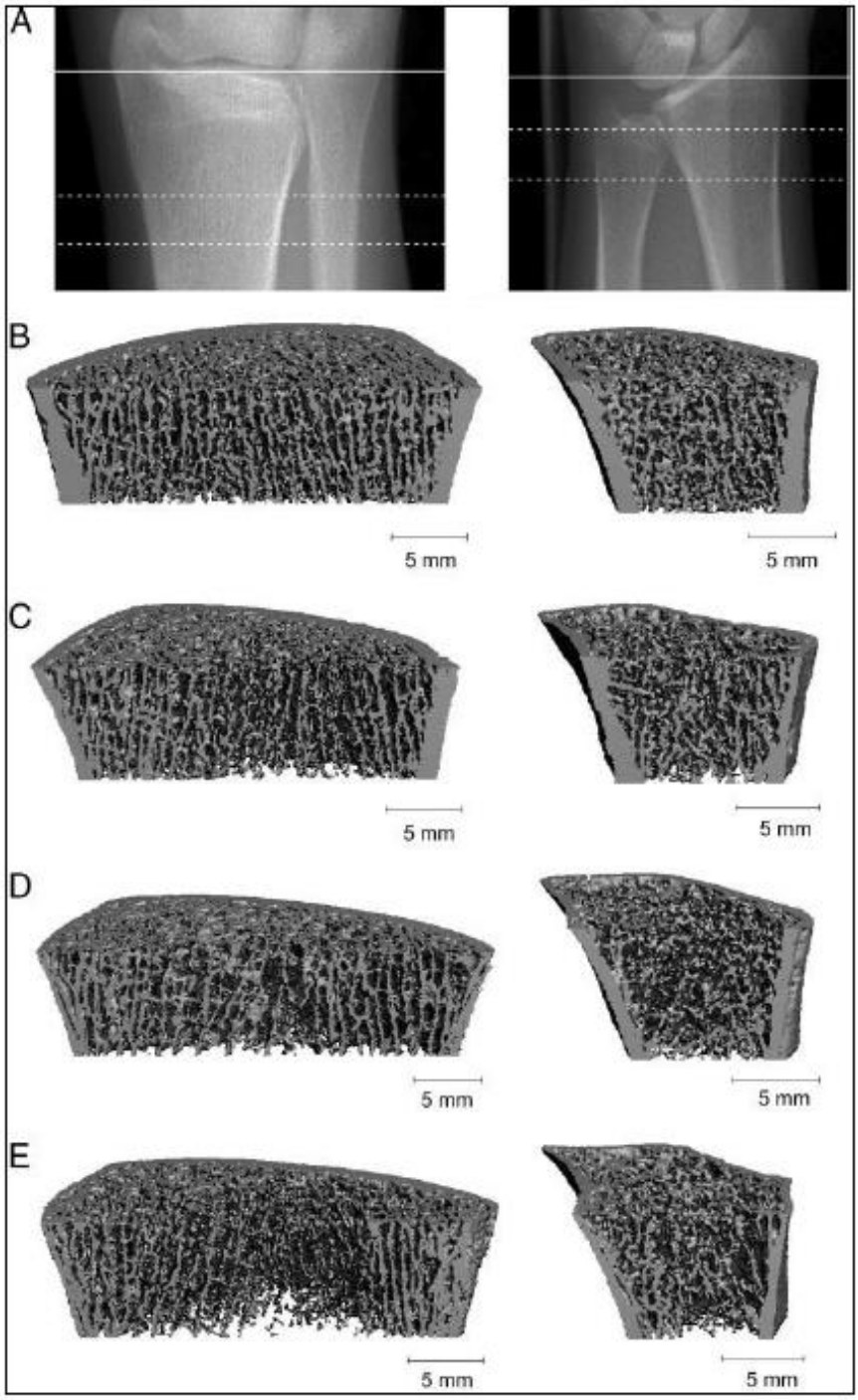

Figure 30 Images of the tibia(left)and radius (right). A. View demonstrating the reference line (solidline) and the measurement site (between dotted lines); B-E, images from a premenopausal (b), postmenopausal osteopenic (C), postmenopausal osteoporotic (D), and postmenopausal severe osteoporotic (E) subject. [45]

Animal models are often used to better understand diseases and possible

treatments. For osteoporosis research it is imperative that the animal exhibit osteoporotic

characteristics. An ovariectomy surgery, involving the removal of the ovaries, is used to simulate osteopenia in animals. It has shown to an effective treatment in many different animal models, showing osteoporotic characteristics such as increased bone turnover that then leads to bone loss [27]. This treatment allows for a useful model of not only osteoporosis, but of postmenopausal osteoporosis as well. Rat models having undergone ovariectomies show alteration in cancellous bone that is identical to the bone loss seen in humans during aging and menopause [46]. Other animal models that have shown reduction in cancellous bone due to ovariectomies include primates and sheep.

When initially testing the pathophysiology of bone loss, menopause, and the proposed therapy options, small animals such as rats and mice are the preferred animal model. Smaller animals are preferred due to having advantages over larger animal models in being much more cost effective. There are drawbacks to using a smaller animal model including differences in biomechanical bone characteristics, hormone profiles, and reproductive physiology causing a less accurate simulation of human osteoporosis. Smaller animal models also lack the size to test implantable devices interactions with bone tissue undergoing bone loss [47]. As mentioned above primates are another animal model that has obvious advantages of being a more suitable animal model due to their closer similarities in hormonal profiles, anatomies, and size to humans. The main disadvantages to utilizing primates as a plausible animal model are the difficulty of handling, needing older primates, and having an extremely higher cost [27].

Taking into account the disadvantages to using a rat and primate model, a sheep animal model is a well suited option for analysis of postmenopausal osteoporosis for many reasons. Some of the advantages to utilizing a sheep model are that sheep show

bone loss with estrogen depletion, have similar hormone profiles compared to human females, and have similar Haversian remodeling. One noticeable drawback to using sheep as an optimal model is the fact that some breeds are seasonally polyestrous and have periods of anestrus, where the animal naturally undergoes estrogen depletion [29]. This is the largest difference between the human model and the sheep model. However, this has been taken into consideration and the effects of seasonality have been studied in another portion of this animal study on the effects of estrogen depletion on bone remodeling.

Along with seasonality a few other important factors have not been assessed in using a sheep model for the study of post-menopausal osteoporosis. These include findings of possible variation due to anatomical sector in bone and effective amount of time post ovariectomy to begin to show statistical changes in resorption surfaces, osteoblast surfaces, bone formation rates, and bone mass. Previous studies have used sheep as a better model of osteoporosis using the parameters mentioned above, but measured over a period of 18 months [31]. This however does not account for possible changes in earlier remodeling cycles as well as for anatomical sectors of bone. It is known that the resorption and remodeling process takes roughly 3 months to complete [7]. So it is reasonable to believe some noticeable changes may occur after one remodeling cycle post ovariectomy. One study has shown that 3 months after ovariectomy surgery there was a statistical difference seen in resorption surface, osteoblast surface and bone formation values, but a change in BMD was not seen until 6months [34]. This study also did not account for any variation due to anatomical region in the cross section of the bone.

There are a number of reasons why taking into account the possible variation due

to anatomical region would be useful in the study of the effects of osteoporosis on bone remodeling. Bone undergoes a multitude of stresses during activity. In particular the caudal cortex of bone in the leg is in compression and the cranial cortex is in tension with lower stresses in the lateral and medial sections of bone [48]. With different anatomical regions of bone undergoing different types of strains it would be a reasonable suggestion to study the effects of osteoporosis on different anatomical regions of bone. One study has shown that there was in fact, a statistically significant variation in bone mineralization between anatomical regions of a cross section of bone [49].

In this study we looked to see if there were noticeable changes to the bone after one remodeling cycle, there was a significant effect on data in this study due to anatomical sector. Analysis of the OVX and control data on 3 month summer sheep showed variation at the caudal sector 5 location for fraction remodeled material and the mean osteon area. The significant variation seen was expected due to the different load types experienced by each sector. The control sheep showed a significantly higher fraction of remodeled material than that of the OVX sheep. In order for this to happen, the OVX sheep would need to be modeling bone, which would show up as unremodeled bone or that the OVX sheep had a lower amount of remodeled bone at the time of surgery than that of the control sheep. The significant variation seen in the mean area of osteons in sector 5 supports this assumption that the control sheep had a greater amount of remodeled tissue. The control sheep had significantly larger Osteons as compared to that of the OVX sheep. This could possibly be due to the expected post-OVX remodeling burst creating smaller osteons. It is understandable to see the most variation in sector 5, as it is the most active region of the bone, the caudal region corresponds to an area of

high compression [50]. The samples used were taken from a 1.5mm x 1.5mm beam in sector 5. It may be considered that due to the high variation in bone properties in this region of the bone, the sample size taken from sector 5 may be too small to get a varied enough sample size of bone to come to any definitive conclusions. A significant variation was also seen in the average osteons per mm^2 of the remodeled material in sector 6. The control sheep showed a higher average of osteons per mm^2 than the OVX sheep, the control sheep also had a significantly larger Standard Deviation than OVX. This can be attributed to the fact that the ulna is adjacent to sector 6 and could have been in a fusing process with the radius in some of the control sheep causing the increased variability seen. It should also be noted that the mean osteonal area found was about half what you would expect with osteons having an average diameter of 200 μm. This could be due to the fact that calculation used osteons per mm^2, however, many osteons overlap causing the calculated mean area to be less than expected. Significant variations in the other parameters tested during this study were not seen between the control and OVX sheep as well as between the anatomical sectors of bone. This was expected, because of the minimal remodeling that could occur within 3 months of the ovariectomy surgery.

Significant variation in the equivalent thickness of aluminum (ETA) was seen between the control and OVX sheep at the 3 month time point. A time period of 3 months has shown to be a long enough period post ovariectomy to see significant change in the density of the bone. This shows that there could be a substantial increase in the resorption of bone as compared to pre-ovariectomy bone due to estrogen depletion and the increase in osteoclastogenesis. There was no significant variation seen between sectors and was seen as an overall decrease in ETA between OVX sheep and control sheep.

There were a few limitations to this study including the purchase cohort effect. This is relevant to the study because the sheep that where purchased were already skeletally mature as a result of previous remodeling cycles experienced before their arrival at Colorado State University. This effect was minimized by maintaining a uniformity of where the sheep were housed and by giving them the same feed and exercise conditions during their post-operative time. Time in these conditions was also taken into account and was most optimal for the 12 month sheep and understandably restrained for the 3 month sheep.

Another constraint that was found during this study was the projection of the 3D structure of the bone samples onto a 2D plane, as seen in the microradiographs. With the projection of the 3D structure onto a 2D plane, the density of the sample may interfere with the dimensions of the features being measured on the microradiographs. This poses a problem when making histomorphometric measurements from the microradiographs without optimal accuracy, however with the samples being of 100 microns in size this should be minimal at the most. Along with the issues of projecting a 3D feature onto a 2D plane, there were a few issues with obtaining optimal exposure on the microradiographs. The issues with exposure caused low visibility on a number of the specimens creating difficulty in obtaining the most accurate histomorphometric measurements. The exposure issues also played a role in the densitometry measurements. The main issue being that some sectors would be over exposed (too bright) or that some would be under exposed (to dark). This was partially resolved by changing the lighting during image retrieval to optimize visualization of the images to be used in creating the sigmoidal curves.

With the results found from this study, there can potentially be many more studies done to further increase the understanding of the effects of estrogen depletion on bone remodeling. One such area that is of interest is to study if the effects of seasonality have any effect on 3 month ovariectomized sheep. Also we can further study the effects of estrogen and other drug therapies on osteoporotic bone using an OVX sheep model that takes into account seasonality and anatomical sector of bone. This would aid in better understanding where these treatments affect such parameters as BMD, resorption surfaces, osteoblast surfaces, and bone formation rates as compared to non-treated OVX sheep.

With the OVX data collected it is apparent that there were significant variations in parameters in bone remodeling seen in specific sectors even 3 months post-surgery. It was also seen that there was a significant difference in bone density at this same time point. With this knowledge we can see that different anatomical regions are not affected by bone loss equivalently, but rather increased based on the amount of stress associated with that region. As a result, it is important for protocols of future studies to take into account, not only the treatments but also the anatomical regions and time period of analysis. This research has shown that there are many different levels of remodeling seen in the adult OVX ovine model, shows that this is a useful model for post-menopausal osteoporosis for 3 month OVX sheep, and that an ovariectomy does have significant effect on bone remodeling for a 3 month post-op ovine model.

5. Conclusion

The use of an ovariectomized adult ewe can provide an economical large animal model for studies of postmenopausal osteoporosis and compact bone remodeling. Using a sheep as the animal model offers many advantages over other possible animal models. Sheep have shown that they exhibit similar Haversian remodeling to humans due to similar hormonal, exercise, and dietary changes. Along with showing similar bone remodeling they offer a large animal model that implant devices can be tested as treatment methods. With ovariectomized sheep showing similar effects on remodeling as seen during menopause in human women, it makes it an ideal model for postmenopausal osteoporosis studies.

The sheep model used in this portion of the research involved the use of 2 groups of sheep, ovariectomized sheep and control sham surgery sheep, which both underwent surgery in the summer and were sacrificed at 3 months post-surgery. The procedures and handling of the sheep took place at Colorado State University where after sacrifice the sheep's right and left radius and ulna bone were removed and sent to Henry Ford Hospital for further preparation and analysis. Once at the Henry Ford Hospital the left radius and ulna bone were used for mechanical testing. The right radius and ulna bone were cut into a cross section then divided into six anatomical sectors and ground down to a final thickness of 100μm for microradiograph imaging. Along with the bone samples an aluminum step wedge was created and imaged with the bone samples to provide a key for the densitometry analysis to be performed. Once the microradiograph slides were completed, they were sent to California Polytechnic State University, San Luis Obispo for histomorphometric and densitometry analysis.

For the histomophometric analysis portion of this study, the microradiographs of the bone samples taken from the aforementioned sheep were viewed under a white light microscope with overlaying Merz grid. Using the Merz grid the anatomical bone sectors were divided into quadrants for taking measurements. The following measurements were taken to quantify bone remodeling: porosity, remodeled bone, number of secondary osteons, and cement line interfaces. The values taken from each quadrant were averaged for each sector of bone. Using these values, bone remodeling parameters were calculated using a Microsoft Excel spreadsheet. The parameters found were the bone volume to tissue volume ratio (BV/TV), fraction remodeled tissue and bone, the cement line interfaces of tissue and bone, osteons per mm^2, and the mean osteon area.

The densitometry portion of this study required computational images taken of each specimen along with its corresponding aluminum step wedge on the microradiographs. When taking these images, light intensity and exposure rates were kept constant for each specimen and their corresponding step wedge to reduce possible error from variation. These images where then processed using digital image analysis software to measure the light intensity of each pixel on a scale of 0 to 255. This was performed for each sector and each step of the step wedge. Using the mean pixel intensity of each step of the step wedges a key could be determined for a calibration curve. Using the calculated calibration curve found from the step wedges, the mean pixel intensities of the bone specimens could be used to calculate their equivalent thickness of aluminum (ETA) giving us a quantitative value for density of each specimen.

Once all data was collected for the histomorphometry and densitometry of the 3 month OVX and control sheep statistical analysis was then performed. To best analyze

the data a 2-way Repeated Measures ANOVA test was ran for each remodeling parameter and for the ETA's. The ANOVA model performed allowed for the comparison in the difference seen in treatment (OVX vs. control), sector (anatomical sectors 1-6), and the combination of sectors and test. The histomorphic data showed a significant variation in sector 5 between OVX and control sheep for the fraction of remodeled material and bone where the control sheep in sector 5 showed a significantly higher fraction of remodeled material and bone than that of the OVX sheep in sector 5. A significant variation was also seen in sector 6 between OVX and control sheep for the average osteon per field, where the control sheep showed a significantly higher amount of osteons per mm^2 than that of the OVX sheep. There were no significant differences seen in any of the other parameters between treatments for sectors. For the densitometry statistical analysis there was a significant difference seen between test specimens where the OVX sheep had significantly lower ETA's than that of the control sheep. There were no significant differences seen between individual sectors.

The significant variations in cortical bone remodeling seen at only 3 months post ovariectomy show that it is important to take into account the possible variations seen in the early stages of bone remodeling and the significant variance seen between anatomical sectors using sheep as the animal model, in particular the variation seen in sector 5. It is essential that the findings found in this study be taken into consideration when developing protocols for future research using the ovariectomized adult ewe as a model for post-menopausal osteoporosis and its possible treatments. For future research it should be considered to increase the sample size used. If unable to increase the number of animals used in the study it may be beneficial to take multiple samples from regions with

the most variation to increase your sample size This study shows that an ovariectomized sheep model can be a very useful model of postmenopausal osteoporosis and that variations caused by follow up times and anatomical sectors must be taken into account to get an even clearer interpretation of results found in future studies.

References

1. WHO, *WHO Scientific Group on the Assessment of Osteoporosis at Primary Health Care Level*. 2004: Brussels.
2. Ammann, P. and R. Rizzoli, *Bone strength and its determinants.* Osteoporosis Int, 2003. 14 Suppl 3: p. S13-8.
3. NOF. *National Osteoporosis Foundation: Fast Facts*. Available from: http://www.nof.org/node/40.
4. Poole, K.E.S. and J.E. Compston, *Osteoporosis and its management.* BMJ, 2006. 333(7581): p. 1251-1256.
5. Ethier, C. Ross and Simmons, Craig A., *Introductory Biomechanics: From Cells to Organisms*. 2007: Cambridge University Press
6. Martin, R.B., D.B. Burr, and N.A. Sharkey, *Skeletal tissue mechanics*. 1998: Springer.
7. Bilezikian, J.P., L.G. Raisz, and T.J. Martin, *Principles of bone biology*. 2008: Elsevier.
8. Nordin, M. and V.H. Frankel, *Basic biomechanics of the musculoskeletal system*. 2001: Lippincott Williams & Wilkins.
9. Young, M.F., *Bone matrix proteins: their function, regulation, and relationship to osteoporosis.* Osteoporos Int, 2003. 14 Suppl 3: p. S35-42.
10. Buchman, S.R., et al., *Use of microcomputed tomography scanning as a new technique for the evaluation of membranous bone.* The Journal of craniofacial surgery, 1998. 9(1): p. 48-54.
11. Seeman, E. and P.D. Delmas, *Bone quality--the material and structural basis of bone strength and fragility.* N Engl J Med, 2006. 354(21): p. 2250-61.
12. Eriksen, E.F., et al., *Reconstruction of the formative site in iliac trabecular bone in 20 normal individuals employing a kinetic model for matrix and mineral apposition.* Metab Bone Dis Relat Res, 1984. 5(5): p. 243-52.
13. Martin, R.B., *Toward a unifying theory of bone remodeling.* Bone, 2000. 26(1): p. 1-6.
14. Katzenberg, M.A. and S.R. Saunders, *Biological anthropology of the human skeleton*. 2008: Wiley-Liss.
15. Paoletti, Nicola, *Multilevel Computational Modeling and Quantitative Analysis of Bone Remodeling.* IEEE-ACM TRANSACTIONS ON COMPUTATIONAL BIOLOGY AND BIOINFORMATICS, 2012. 9(5): p. 1366-1378.
16. L.Santos, J.C. Romeu, H. Canhao, J.E. Fonseca, P.R. Ferndes, *A quantitative comparison of a bone remodeling model with dual-energy X-ray absorptiometry and analysis of the inter-individual biological variability of femoral neck T-score.* Journal of Biomechanics, 2010. 43(16): p. 3150-3155.
17. Umoh, Joseph U , Sampaio, Arthur V , Ian Welch, Vasek Pitelka, Harvey A Goldberg, T Michael Underhill, David W Holdsworth, *In vivo micro-CT analysisof bone remodeling in a rat calvarial defect model.*Physics in Medicine and Biology, 2009. 54(7): p. 2147-2161.
18. Abbott Iii, T.A., B.J. Lawrence, and S. Wallach, *Osteoporosis: the need for comprehensive treatment guidelines.* Clinical Therapeutics, 1996. 18(1): p. 127-149.
19. Fazzalari, N.L., *Bone remodeling: A review of the bone microenvironment perspective for fragility fracture (osteoporosis) of the hip.* Semin Cell Dev Biol, 2008. 19(5): p. 467-72.
20. Demir, B., et al., *Identification of the risk factors for osteoporosis among postmenopausal women.*Maturitas, 2008. 60(3–4): p. 253-256.
21. Nelson, H.D., et al., *Osteoporosis and Fractures in Postmenopausal Women Using Estrogen.* Arch Intern Med, 2002. 162(20): p. 2278-2284.
22. Jilka, R.L. *Cytokines, bone remodeling, and estrogen deficiency: a 1998 update.* Bone, 1998. 23(2):p. 75-81.

23. Delmas, P.D., *Treatment of postmenopausal osteoporosis.* The Lancet, 2002. 359(9322): p. 2018-2026.
24. Ego, S., *Osteoporosis: Trials and tribulations.* The American Journal of Medicine, 1997. 103(2, Supplement 1): p. S74-S89.
25. Manolagas, S.C., *Birth and death of bone cells: basic regulatory mechanisms and implications for the pathogenesis and treatment of osteoporosis.* Endocr Rev, 2000. 21(2): p. 115-37.
26. Turner, A.S., *Seasonal changes in bone metabolism in sheep: further characterization of an animal model for human osteoporosis.* Vet J, 2007. 174(3): p. 460-1.
27. Turner, A.S., *Animal models of osteoporosis--necessity and limitations.* Eur Cell Mater, 2001. 1: p. 66- 81.
28. Feher, A., et al., *Bisphosphonates do not inhibit periosteal bone formation in estrogen deficient animals and allow enhanced bone modeling in response to mechanical loading.* Bone, 2010. 46(1): p. 203-207.
29. Newman, E., A.S. Turner, and J.D. Wark, *The potential of sheep for the study of osteopenia: current status and comparison with other animal models.* Bone, 1995. 16(4 Suppl): p. 277S-284S.
30. Baofeng, L., et al., *Characterization of a rabbit osteoporosis model induced by ovariectomy and glucocorticoid.* Acta Orthopaedica. 81(3): p. 396-401.
31. Arens, D., et al., *Seasonal changes in bone metabolism in sheep.* Vet J, 2007. 174(3): p. 585-91.
32. Newton, B.I., et al., *The Ovariectomized Sheep as a Model for Human Bone Loss.* Elsevier, 2004. 130: p. 323-326.
33. Turner, A.S., *The sheep as a model for osteoporosis in humans.* Vet J, 2002. 163(3): p. 232-9.
34. Turner, A.S., et al., *Changes in bone mineral density and bone-specific alkaline phosphatase in ovariectomized ewes.* Bone, 1995. 17(4 Suppl): p. 395S-402S.
35. Wu, Z.-x., et al., *Effect of ovariectomy on BMD, micro-architecture and biomechanics of cortical and cancellous bones in a sheep model.* Medical Engineering & Physics, 2008. 30(9): p. 1112-1118.
36. Lill, C.A., A.K. Fluegel, and E. Schneider, *Effect of ovariectomy, malnutrition and glucocorticoid application on bone properties in sheep: a pilot study.* Osteoporos Int, 2002. 13(6): p. 480-6.
37. Calcagno, J., *Seasonal and Anatomical Variation in Compact Bone Remodeling in the Adult Bone*, in *Biomedical Engineering*. 2011, California Polytechnic State Univeristy: San Luis Obispo. p. 134.
38. Boivin, G. and P.J. Meunier, *The degree of mineralization of bone tissue measured by computerized quantitative contact microradiography.* Calcif Tissue Int, 2002. 70(6): p. 503-11.
39. Parfitt, A.M. Chapter 5: Stereologic basis of Bone Histomorphometry; Theory of Quantitative Microscopy and Reconstruction of the Third Dimension. In: Recker, R.R.(Ed.), Bone Histomorphometry: Techniques and Interpretation. CRC Press, Boca Raton, FL. Pp.(52-87), 1983
40. Yates, A.J., et al., *Radiographic absorptiometry in the diagnosis of osteoporosis.* The American Journal of Medicine, 1995. 98(2, Supplement 1): p. 41S-47S.
41. Parsons, L.C., *Osteoporosis: Incidence, Prevention, and Treatment of the Silent Killer.* Nursing Clinics of North America, 2005. 40(1): p. 119-133.
42. Ruan, W.-d., et al., *Analysis on the risk factors of second fracture in osteoporosis-related fractures.* Chinese Journal of Traumatology (English Edition), 2011. 14(2): p. 74-78.

43. Augat, P., et al., *Osteoporosis prevalence and fracture characteristics in elderly female patients with fractures.* Archives of Orthopaedic and Trauma Surgery, 2010. 130(11): p. 1405-1410.
44. Lespessailles, E., et al., *Imaging techniques for evaluating bone microarchitecture.* Joint Bone Spine, 2006. 73(3): p. 254-61.
45. Boutroy, S., et al., *In Vivo Assessment of Trabecular Bone Microarchitecture by High-Resolution Peripheral Quantitative Computed Tomography.* Journal of Clinical Endocrinology & Metabolism, 2005. 90(12): p. 6508-6515.
46. Mosekilde, L., *Assessing bone quality — Animal models in preclinical osteoporosis research.* Bone, 1995. 17(4, Supplement): p. S343-S352.
47. Thorndike, E.A. and A.S. Turner, *In search of an animal model for postmenopausal diseases.* Front Biosci, 1998. 3: p. c17-26.
48. Biewener, Andrew A., C. Richard Taylor, *Bone Strain: A Determinant of Gait and Speed?.* J Exp Biol, 1986. 123: p. 383-400.
49. Rohrbach, Daniel , Laksjmanan, Sannachi, Peyrin, Francoise, Langer, Max, Gerisch, Alf, Grimal, Quentin, Laugier, Pascal, Raum, Kay, *Spatial distribution of tissue level properties in a human femoral cortical bone.* Journal of Biomechanics, 2012. 45(13): p.2264-2270
50. Lanyon, L.E., P.T. Magee, and D.G. Baggott, *The relationship of functional stress and strain to the processes of bone remodelling. An experimental study on the sheep radius.* Journal of Biomechanics, 1979. 12(8): p. 593-600.

Appendix A : 3 Month Summer OVX Histomorphometry Data

3 Month Summer OVX						
Average BV/TV						
	Sector					
Sheep	**Craniomedial**	**Cranial**	**Craniolateral**	**Caudomedial**	**Caudal**	**Caudolateral**
C02	0.938	0.944	0.951	0.840	0.972	0.935
C09	0.944	0.986	0.986	0.958	0.972	0.972
C12	0.926	0.958	0.972	0.938	0.944	0.972
C14	0.972	0.965	0.917	0.979	0.958	0.979
C19	0.954	0.979	0.944	0.972	0.944	0.986
C20	0.965	0.963	0.938	0.938	0.951	0.951
C21	0.965	0.944	0.993	0.979	0.903	
C25	0.986	0.993	0.917	0.979	1.000	0.944
Average Fraction Remodeled (Tissue)						
	Sector					
Sheep	**Craniomedial**	**Cranial**	**Craniolateral**	**Caudomedial**	**Caudal**	**Caudolateral**
C02	0.542	0.382	0.618	0.424	0.444	0.509
C09	0.479	0.438	0.417	0.285	0.491	0.347
C12	0.454	0.431	0.521	0.500	0.382	0.424
C14	0.431	0.514	0.417	0.438	0.438	0.319
C19	0.454	0.521	0.563	0.590	0.569	0.535
C20	0.368	0.361	0.549	0.396	0.500	0.375
C21	0.486	0.410	0.563	0.611	0.597	
C25	0.306	0.417	0.269	0.444	0.521	0.361
Average Fraction Remodeled (Material)						
	Sector					
Sheep	**Craniomedial**	**Cranial**	**Craniolateral**	**Caudomedial**	**Caudal**	**Caudolateral**
C02	0.577	0.404	0.649	0.502	0.457	0.545
C09	0.508	0.442	0.421	0.297	0.505	0.354
C12	0.488	0.449	0.536	0.528	0.404	0.437
C14	0.443	0.534	0.454	0.447	0.456	0.326
C19	0.475	0.531	0.595	0.608	0.604	0.542
C20	0.382	0.375	0.586	0.422	0.526	0.393
C21	0.504	0.435	0.567	0.625	0.657	
C25	0.311	0.420	0.295	0.455	0.521	0.381

Average Cement Line Interface (Tissue) (mm/mm^2)						
	Sector					
Sheep	**Craniomedial**	**Cranial**	**Craniolateral**	**Caudomedial**	**Caudal**	**Caudolateral**
C02	48.11	31.68	45.94	36.43	38.02	35.38
C09	38.61	40.00	40.00	32.67	51.74	32.87
C12	40.92	40.19	49.10	39.80	40.39	41.58
C14	48.31	53.06	43.16	51.88	41.58	34.06
C19	42.24	35.44	47.12	58.81	55.04	52.47
C20	44.35	34.32	38.41	36.04	45.94	37.42
C21	47.72	38.61	42.77	43.36	39.60	
C25	27.92	34.85	19.27	36.43	40.79	32.87
Average Cement Line Interface (Material) (mm/mm²)						
	Sector					
Sheep	**Craniomedial**	**Cranial**	**Craniolateral**	**Caudomedial**	**Caudal**	**Caudolateral**
C02	51.24	33.59	48.28	33.53	39.15	37.81
C09	40.95	40.53	40.51	34.02	53.22	33.56
C12	44.09	41.88	50.44	42.37	42.77	42.77
C14	49.72	55.17	46.91	52.93	43.58	34.83
C19	44.44	36.13	49.97	60.46	58.22	53.38
C20	46.11	35.60	41.23	38.56	48.26	39.34
C21	49.48	40.94	43.10	44.34	43.92	
C25	28.34	35.11	21.32	37.18	40.79	34.87
Average Cement Line Interface (Remodeled Material) (mm/mm²)						
	Sector					
Sheep	**Craniomedial**	**Cranial**	**Craniolateral**	**Caudomedial**	**Caudal**	**Caudolateral**
C02	90.67	83.78	75.12	67.70	88.97	70.46
C09	80.68	95.49	101.74	116.21	106.19	95.25
C12	93.37	93.66	94.15	82.17	105.35	100.84
C14	114.04	103.22	106.60	119.44	96.27	107.95
C19	95.04	66.49	85.33	101.34	96.87	99.92
C20	122.22	95.81	72.51	91.92	96.11	105.14
C21	99.12	95.60	76.16	70.90	67.45	
C25	96.48	84.48	71.60	83.44	78.70	93.74

Osteons/mm² (Tissue)						
	Sector					
Sheep	**Craniomedial**	**Cranial**	**Craniolateral**	**Caudomedial**	**Caudal**	**Caudolateral**
C02	43.25	30.25	26.50	27.25	31.33	35.00
C09	29.50	44.50	32.75	33.25	41.00	32.75
C12	35.00	32.50	32.25	27.00	27.75	27.50
C14	44.25	29.00	27.25	38.25	28.50	29.75
C19	48.33	30.00	31.50	33.75	39.50	39.00
C20	29.50	31.33	33.50	46.00	35.50	42.00
C21	37.00	26.25	30.75	23.50	27.00	
C25	34.25	23.50	16.33	25.00	25.25	19.50
Osteons/mm² (Material)						
	Sector					
Sheep	**Craniomedial**	**Cranial**	**Craniolateral**	**Caudomedial**	**Caudal**	**Caudolateral**
C02	46.06	32.04	27.88	32.48	32.23	37.44
C09	31.26	45.05	33.20	34.68	42.17	33.59
C12	37.72	33.89	33.13	28.69	29.38	28.28
C14	45.53	30.17	29.59	39.06	29.73	30.41
C19	50.83	30.61	33.42	34.74	41.72	39.68
C20	30.63	32.54	35.69	49.05	37.31	44.24
C21	38.31	27.79	30.99	23.97	30.09	
C25	34.70	23.66	17.99	25.54	25.25	20.68
Osteons/mm² (Remodeled Material)						
	Sector					
Sheep	**Craniomedial**	**Cranial**	**Craniolateral**	**Caudomedial**	**Caudal**	**Caudolateral**
C02	81.63	80.82	43.07	66.17	75.00	69.68
C09	62.13	103.24	84.73	118.34	84.99	99.34
C12	79.63	75.73	61.91	55.27	72.01	67.45
C14	104.18	56.60	67.03	88.28	65.62	93.93
C19	109.50	58.63	56.53	57.99	69.60	74.18
C20	81.00	88.14	63.36	116.43	74.58	123.94
C21	78.38	65.62	54.73	38.58	46.44	
C25	125.14	57.80	60.80	57.86	48.94	55.53

Mean Osteon Area (microns^2)						
	Sector					
Sheep	**Craniomedial**	**Cranial**	**Craniolateral**	**Caudomedial**	**Caudal**	**Caudolateral**
C02	12525.46	12734.89	23505.89	15710.55	14702.51	14581.39
C09	16394.98	9747.72	12649.81	8738.49	11950.40	10396.34
C12	13149.49	13254.08	16292.58	18469.26	14107.48	16199.57
C14	9740.09	17802.82	15580.48	11555.42	15401.52	10796.80
C19	9423.87	17169.52	17967.57	17601.17	14646.46	14087.89
C20	12408.40	11453.66	16713.66	8605.96	14502.17	9103.65
C21	13645.78	15636.02	18500.98	26594.26	22119.34	
C25	9112.29	18375.28	16486.63	17870.37	20956.48	18603.80

Appendix B: 3 Month Summer Control Histomorphometry Data

3 Month Summer Control						
Average BV/TV						
	Sector					
Sheep	**Craniomedial**	**Cranial**	**Craniolateral**	**Caudomedial**	**Caudal**	**Caudolateral**
C15	0.958	0.986	0.981	0.986	0.958	0.993
C16	0.965	0.972	0.951	0.958	0.924	0.965
C17	0.944	0.951	0.944	0.979	0.958	0.986
C23	0.944	0.954	0.979	0.986	0.986	0.951
C24	0.972	0.979	0.958	0.986	0.764	0.965
C27	0.986	0.965	0.993	0.958	0.958	0.944
C28	0.965	0.958	0.951	0.944	0.958	0.972
C29	0.972	0.958	0.979	0.951	0.986	0.979
Average Fraction Remodeled (Tissue)						
	Sector					
Sheep	**Craniomedial**	**Cranial**	**Craniolateral**	**Caudomedial**	**Caudal**	**Caudolateral**
C15	0.347	0.389	0.426	0.514	0.438	0.410
C16	0.347	0.444	0.403	0.625	0.611	0.521
C17	0.354	0.500	0.424	0.458	0.708	0.375
C23	0.542	0.370	0.493	0.549	0.576	0.347
C24	0.410	0.493	0.486	0.417	0.507	0.486
C27	0.396	0.333	0.444	0.410	0.535	0.167
C28	0.319	0.431	0.479	0.389	0.590	0.083
C29	0.375	0.368	0.535	0.458	0.576	0.361
Average Fraction Remodeled (Material)						
	Sector					
Sheep	**Craniomedial**	**Cranial**	**Craniolateral**	**Caudomedial**	**Caudal**	**Caudolateral**
C15	0.362	0.393	0.434	0.521	0.456	0.412
C16	0.359	0.457	0.422	0.652	0.660	0.539
C17	0.375	0.527	0.448	0.468	0.739	0.381
C23	0.573	0.389	0.505	0.557	0.584	0.365
C24	0.421	0.503	0.510	0.423	0.666	0.504
C27	0.402	0.345	0.447	0.428	0.558	0.177
C28	0.332	0.448	0.503	0.412	0.613	0.086
C29	0.385	0.384	0.546	0.481	0.584	0.369

Average Cement Line Interface (Tissue) (mm/mm^2)						
	Sector					
Sheep	**Craniomedial**	**Cranial**	**Craniolateral**	**Caudomedial**	**Caudal**	**Caudolateral**
C15	31.68	40.00	48.31	46.93	48.91	35.84
C16	37.62	36.83	39.80	60.19	44.55	40.19
C17	40.00	41.98	40.79	54.85	60.19	37.82
C23	44.15	25.87	41.38	43.76	38.61	29.70
C24	34.85	43.76	44.35	43.16	38.81	48.31
C27	34.45	29.70	25.34	37.42	51.68	13.07
C28	39.60	38.61	46.33	35.84	45.74	11.48
C29	39.20	31.48	50.09	37.22	45.54	33.46
Average Cement Line Interface (Material) (mm/mm^2)						
	Sector					
Sheep	**Craniomedial**	**Cranial**	**Craniolateral**	**Caudomedial**	**Caudal**	**Caudolateral**
C15	32.99	40.50	49.30	47.62	51.20	36.07
C16	39.03	38.07	42.12	62.74	47.99	41.53
C17	42.50	44.05	43.26	56.02	62.75	38.37
C23	46.83	27.21	42.26	44.37	39.17	31.08
C24	35.84	44.58	46.21	43.72	51.23	50.06
C27	34.94	30.55	25.44	39.14	53.94	13.66
C28	41.09	40.17	48.68	37.97	47.50	11.81
C29	40.25	32.87	51.10	39.24	46.18	34.16
Average Cement Line Interface (Remodeled Material) (mm/mm^2)						
	Sector					
Sheep	**Craniomedial**	**Cranial**	**Craniolateral**	**Caudomedial**	**Caudal**	**Caudolateral**
C15	93.72	105.02	113.26	91.78	113.75	88.87
C16	110.74	86.99	102.28	96.21	72.50	76.93
C17	114.10	84.36	96.67	120.14	85.14	100.93
C23	82.74	69.21	85.35	80.32	68.34	87.10
C24	85.37	88.43	96.60	108.28	76.26	104.59
C27	89.03	89.39	56.28	91.93	100.36	78.41
C28	125.45	89.93	97.08	95.08	78.08	163.94
C29	106.40	85.69	93.10	83.66	79.14	95.87

Osteons/mm² (Tissue)						
	Sector					
Sheep	**Craniomedial**	**Cranial**	**Craniolateral**	**Caudomedial**	**Caudal**	**Caudolateral**
C15	35.75	51.75	36.33	27.75	39.50	34.00
C16	43.50	24.50	30.75	37.75	34.50	37.00
C17	44.25	24.25	41.25	48.00	32.50	32.25
C23	32.75	23.67	35.50	25.00	23.00	29.00
C24	46.75	35.00	39.50	41.50	19.75	40.50
C27	33.00	28.25	23.00	27.50	33.50	16.00
C28	40.50	24.00	35.75	29.75	30.75	33.50
C29	48.75	23.25	30.50	33.25	26.25	21.75
Osteons/mm² (Material)						
	Sector					
Sheep	**Craniomedial**	**Cranial**	**Craniolateral**	**Caudomedial**	**Caudal**	**Caudolateral**
C15	37.25	52.49	37.04	28.14	41.34	34.23
C16	45.02	25.22	32.34	39.45	37.25	38.28
C17	46.89	25.55	43.72	49.01	33.88	32.69
C23	34.72	24.83	36.29	25.32	23.31	30.51
C24	48.09	35.72	41.27	42.01	25.82	41.95
C27	33.51	29.25	23.15	28.74	34.94	16.63
C28	41.98	25.05	37.63	31.52	32.07	34.46
C29	50.17	24.30	31.10	35.08	26.64	22.22
Osteons/mm² (Remodeled Material)						
	Sector					
Sheep	**Craniomedial**	**Cranial**	**Craniolateral**	**Caudomedial**	**Caudal**	**Caudolateral**
C15	107.19	139.24	85.20	54.28	91.27	83.91
C16	128.88	56.09	78.15	60.73	56.35	70.86
C17	125.44	48.50	98.76	105.13	45.97	86.35
C23	62.40	65.96	73.78	45.99	40.37	84.73
C24	114.67	71.14	84.87	113.68	39.09	87.06
C27	83.65	85.65	52.63	67.94	66.00	96.00
C28	129.00	56.09	75.27	79.79	53.82	459.00
C29	132.53	63.40	56.49	74.57	45.96	61.94

Mean Osteon Area (microns^2)						
	Sector					
Sheep	**Craniomedial**	**Cranial**	**Craniolateral**	**Caudomedial**	**Caudal**	**Caudolateral**
C15	10096.70	7536.85	11756.92	18526.15	11102.17	12010.63
C16	7930.87	18018.43	13055.20	16788.70	18041.64	14171.12
C17	8035.21	20637.51	10274.97	9587.04	21957.67	11684.37
C23	17890.80	15616.03	13944.93	22300.82	24979.11	12098.16
C24	9006.84	14129.85	12311.62	10155.54	25752.31	12121.21
C27	12047.37	11794.50	19261.23	14982.99	16150.03	12121.21
C28	8092.71	17981.24	13629.85	12957.76	19064.72	2529.76
C29	7715.07	16047.98	17860.58	14282.46	22405.60	16609.55

Appendix C: 3 Month Summer OVX Densitometry Data

3 Month Summer OVX						
Average ETA						
	Sector					
Sheep	**Craniomedial**	**Cranial**	**Craniolateral**	**Caudomedial**	**Caudal**	**Caudolateral**
C02	0.0772	0.0749	0.064	0.0399	0.06	0.0696
C09	0.1042	0.0949	0.0996	0.0678	0.0795	0.0426
C12	0.0844	0.0457	0.0766	0.0622	0.0696	0.0743
C14	0.0814	0.0614	0.0651	0.0618	0.0633	0.0723
C19	0.0615	0.0715	0.0783	0.0859	0.0851	0.0715
C20	0.0765	0.0909	0.0915	0.083	0.0789	0.0817
C21	0.0788	0.0861	0.0878	0.0861	0.0812	
C25	0.0693	0.0833	0.0643	0.0814	0.065	0.0911
Standard Deviation						
	Sector					
Sheep	**Craniomedial**	**Cranial**	**Craniolateral**	**Caudomedial**	**Caudal**	**Caudolateral**
C02	0.01076	0.009479	0.011819	0.0204077	0.020445	0.012876
C09	0.00705	0.007183	0.006794	0.013441	0.009934	0.01506
C12	0.006274	0.013284	0.010155	0.013918	0.009165	0.008771
C14	0.00847	0.007326	0.008933	0.009943	0.022878	0.012552
C19	0.007803	0.007272	0.007206	0.006685	0.007764	0.01182
C20	0.010872	0.007462	0.009074	0.007358	0.011203	0.00807
C21	0.011196	0.006654	0.009375	0.008391	0.004868	
C25	0.00302	0.007047	0.006177	0.013282	0.007864	0.003053
Range						
	Sector					
Sheep	**Craniomedial**	**Cranial**	**Craniolateral**	**Caudomedial**	**Caudal**	**Caudolateral**
C02	0.065359	0.062046	0.057868	0.134553	0.103256	0.08122
C09	0.043222	0.051311	0.054571	0.06355	0.059979	0.069461
C12	0.039973	0.058002	0.05441	0.069214	0.042117	0.055821
C14	0.047125	0.047008	0.052387	0.062442	0.108177	0.078249
C19	0.0367	0.053736	0.043431	0.042139	0.042139	0.066198
C20	0.061507	0.057689	0.06756	0.038493	0.058777	0.045065
C21	0.054399	0.056728	0.068674	0.054843	0.044979	
C25	0.02099	0.079082	0.030558	0.091878	0.096042	0.042572

Appendix D: 3 Month Summer Control Densitometry Data

3 Month Summer Control						
Average ETA						
	Sector					
Sheep	**Craniomedial**	**Cranial**	**Craniolateral**	**Caudomedial**	**Caudal**	**Caudolateral**
C15	0.1031	0.0956	0.0955	0.1023	0.1019	0.1023
C16	0.0799	0.0711	0.081	0.0722	0.0609	0.0891
C17	0.1607	0.1654	0.1657	0.1621	0.1602	0.172
C23	0.0867	0.0779	0.0963	0.08	0.0946	0.0788
C24	0.0869	0.0673	0.0713	0.094	0.0819	0.0692
C27	0.0758	0.0722	0.0828	0.0898	0.0791	0.0939
C28	0.0794	0.0787	0.0603	0.0501	0.0578	0.0995
C29	0.1037	0.097	0.079	0.0956	0.0831	0.1012
Standard Deviation						
	Sector					
Sheep	**Craniomedial**	**Cranial**	**Craniolateral**	**Caudomedial**	**Caudal**	**Caudolateral**
C15	0.008988	0.008385	0.007427	0.009303	0.008618	0.009174
C16	0.009069	0.007501	0.006885	0.008186	0.00783	0.009348
C17	0.014854	0.009085	0.0086	0.011278	0.009348	0.010003
C23	0.007654	0.008737	0.008679	0.009655	0.005927	0.010541
C24	0.010368	0.007763	0.014368	0.00939	0.008186	0.015985
C27	0.010124	0.008157	0.007182	0.006966	0.007768	0.00379
C28	0.008363	0.008457	0.007933	0.010091	0.009308	0.004901
C29	0.007669	0.008603	0.006943	0.00882	0.006606	0.0059
Range						
	Sector					
Sheep	**Craniomedial**	**Cranial**	**Craniolateral**	**Caudomedial**	**Caudal**	**Caudolateral**
C15	0.407696	0.05338	0.045168	0.053155	0.04272	0.055174
C16	0.049275	0.056532	0.039861	0.045023	0.053456	0.055416
C17	0.069684	0.059311	0.044136	0.059439	0.051827	0.069684
C23	0.052901	0.048221	0.050423	0.054988	0.051483	0.056294
C24	0.05121	0.052278	0.074265	0.055475	0.074873	0.082031
C27	0.054527	0.04248	0.063926	0.057717	0.066968	0.042768
C28	0.04383	0.059633	0.048148	0.049122	0.0603067	0.037311
C29	0.049121	0.045595	0.047983	0.049053	0.056394	0.044323